Cell Reports

Article

Sensory neuronal STAT3 is critical for IL-31 receptor expression and inflammatory itch

Graphical abstract

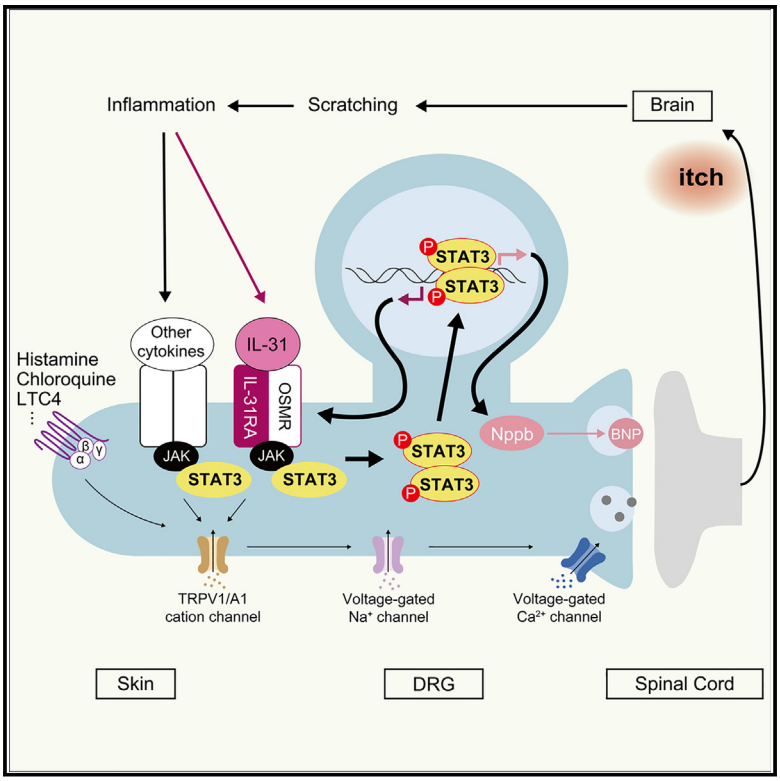

Highlights

- Sensory neuronal IL-31RA and STAT3 are essential for IL-31-induced itch
- STAT3 is important for expression and downstream signaling of IL-31 receptor
- IL-31 enhances GPCR-induced itch transmitted by multiple sensory neuronal subsets
- Sensory neuronal STAT3 contributes to IL-31-independent inflammatory itch

Authors

Sonoko Takahashi, Sotaro Ochiai, Jianshi Jin, ..., Manabu Nakayama, Katsuyuki Shiroguchi, Takaharu Okada

Correspondence

takaharu.okada@riken.jp

In brief

Takahashi et al. demonstrate that sensory neuronal STAT3 is essential for itch, dependent on IL-31, a major pruritogenic cytokine of atopic dermatitis, and further contributes to IL-31-independent itch associated with dermatitis. STAT3 is required for expression and itch-inducing signaling downstream of IL-31 receptor in sensory neurons.

Takahashi et al., 2023, Cell Reports *42*, 113433
December 26, 2023
https://doi.org/10.1016/j.celrep.2023.113433

CellPress

Cell Reports

CellPress
OPEN ACCESS

Article

Sensory neuronal STAT3 is critical for IL-31 receptor expression and inflammatory itch

Sonoko Takahashi,[1,13] Sotaro Ochiai,[1,10,13] Jianshi Jin,[2,11] Noriko Takahashi,[1] Susumu Toshima,[1,3] Harumichi Ishigame,[1,12] Kenji Kabashima,[4,5] Masato Kubo,[6,7] Manabu Nakayama,[8] Katsuyuki Shiroguchi,[2] and Takaharu Okada[1,9,14,*]

[1]Laboratory for Tissue Dynamics, RIKEN Center for Integrative Medical Sciences (RIKEN IMS), Yokohama, Kanagawa 230-0045, Japan
[2]Laboratory for Prediction of Cell Systems Dynamics, RIKEN Center for Biosystems Dynamics Research (RIKEN BDR), Suita, Osaka 565-0874, Japan
[3]Department of Dermatology, Keio University School of Medicine, Tokyo 160-8582, Japan
[4]Department of Dermatology, Kyoto University Graduate School of Medicine, Kyoto 606-8501, Japan
[5]Singapore Immunology Network and Skin Research Institute of Singapore, Agency for Science, Technology and Research, Singapore, Singapore
[6]Laboratory for Cytokine Regulation, RIKEN IMS, Yokohama, Kanagawa 230-0045, Japan
[7]Division of Molecular Pathology, Research Institute for Biomedical Science, Tokyo University of Science, Noda, Chiba 278-0022, Japan
[8]Department of Frontier Research and Development, Kazusa DNA Research Institute, 2-6-7 Kazusa-Kamatari, Kisarazu, Chiba 292-0818, Japan
[9]Graduate School of Medical Life Science, Yokohama City University, Yokohama, Kanagawa 230-0045, Japan
[10]Present address: Malaghan Institute of Medical Research, Wellington 6242, New Zealand
[11]Present address: State Key Laboratory of Integrated Management of Pest Insects and Rodents, Institute of Zoology, Chinese Academy of Sciences, Beijing 100101, P.R. China
[12]Present address: Near InfraRed Photo-Immuno Research Institute, Kansai Medical University, Hirakata, Osaka 573-1010, Japan
[13]These authors contributed equally
[14]Lead contact
*Correspondence: takaharu.okada@riken.jp
https://doi.org/10.1016/j.celrep.2023.113433

SUMMARY

IL-31 receptor blockade suppresses pruritus of atopic dermatitis. However, cell-type-specific contributions of IL-31 receptor to itch, its expression mechanism, and the downstream signaling pathway to induce itch remain unknown. Here, using conditional knockout mice, we demonstrate that IL-31-induced itch requires sensory neuronal IL-31 receptor and STAT3. We find that IL-31 receptor expression is dependent on STAT3 in sensory neurons. In addition, pharmacological experiments suggest that STAT3 activation is important for the itch-inducing signaling downstream of the IL-31 receptor. A cutaneous IL-31 injection induces the nuclear accumulation of activated STAT3 first in sensory neurons that abundantly express IL-31 receptor and then in other itch-transmitting neurons. IL-31 enhances itch induced by various pruritogens including even chloroquine. Finally, pruritus associated with dermatitis is partially dependent on sensory neuronal IL-31 receptor and strongly on sensory neuronal STAT3. Thus, sensory neuronal STAT3 is essential for IL-31-induced itch and further contributes to IL-31-independent inflammatory itch.

INTRODUCTION

Chronic pruritus is a predominant symptom of atopic dermatitis, exacerbates inflammation through scratching, and impairs patients' quality of life. A number of mediators are potentially involved in itch of atopic dermatitis. They directly activate itch-transmitting sensory nerves and/or act on other cell types to promote the production/secretion of other itch mediators. Many of the itch mediators including histamine, leukotrienes, and the mast cell secretagogues are ligands for G protein-coupled receptors (GPCRs).[1,2] Another group of the major itch mediators is the cytokines such as IL-4, IL-13, and IL-31 produced during type 2 inflammation and activating the Janus kinase (JAK)-mediated signaling pathways.[1,2] IL-4 and IL-13 not only act on non-neuronal cells such as immune cells but also activate their receptors expressed by sensory nerves to enhance itch induced by other pruritogens, although these cytokines may not induce strong itch on their own.[3,4] Dupilmab, a monoclonal antibody against the human IL-4/IL-13 receptor, has been shown to alleviate eczema and pruritus of atopic dermatitis though to various extents.[5,6] Unlike IL-4 and IL-13, IL-31 can induce robust itch by itself, although whether IL-31 enhances itch induced by other pruritogens has not been shown.[7,8] The recent clinical trials of nemolizumab, a monoclonal antibody against human IL-31RA, showed that the blockade of IL-31 signaling reduces the intensity of pruritus of atopic dermatitis and prurigo nodularis.[9,10]

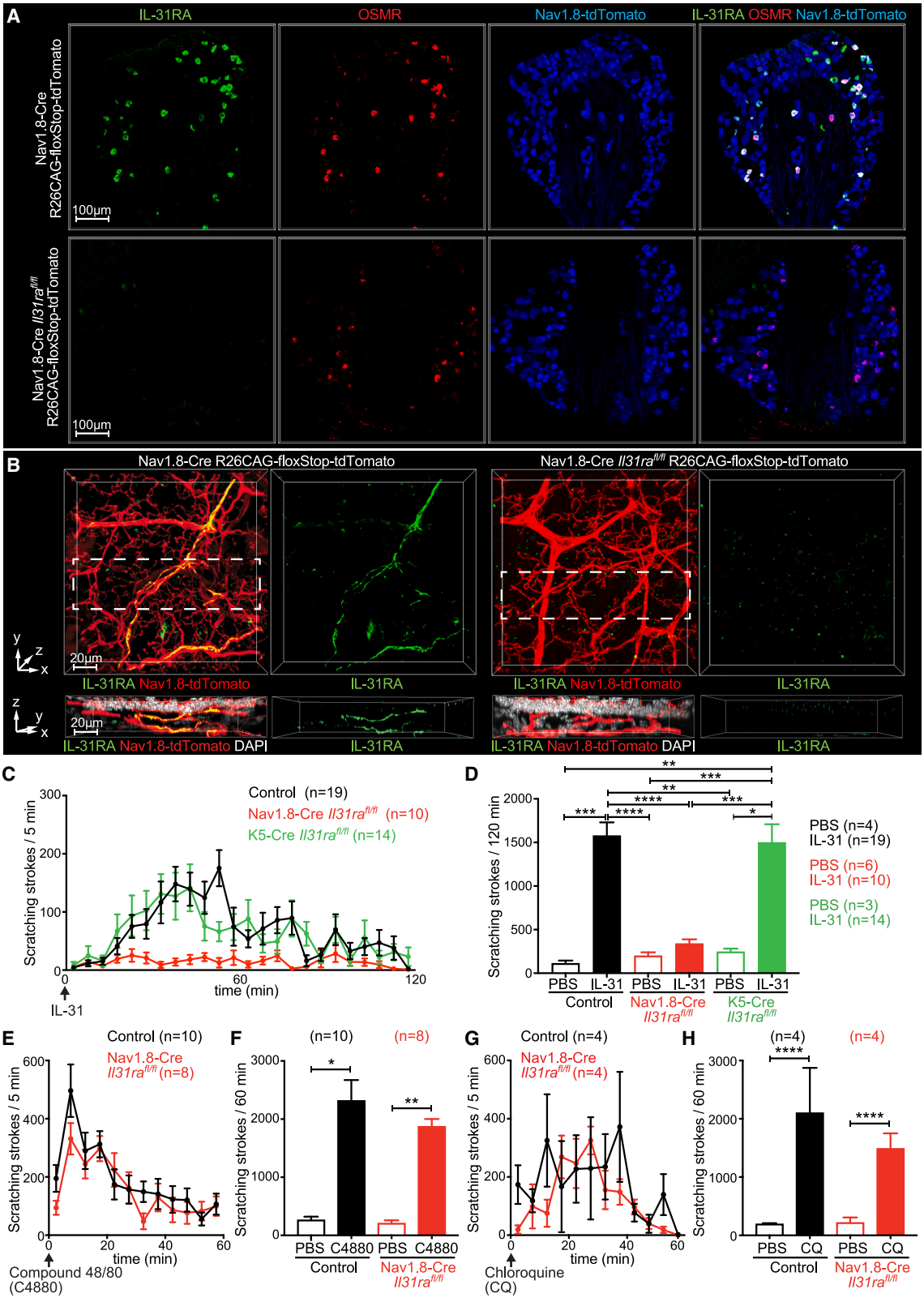

(legend on next page)

IL-31 can be produced by various cell types including T helper type 2 (Th2) cells.[7,8,11] The receptor for IL-31 is composed of two subunits, IL-31RA and oncostatin M receptor (OSMR). IL-31RA is only known to form the IL-31 receptor, while OSMR also forms the receptor for oncostatin M with gp130.[7] Various cell types such as sensory neurons, keratinocytes, and myeloid cells have been reported to express the IL-31 receptor.[7,11] Among sensory neurons in dorsal root ganglia (DRGs), a subset of neurons showed Ca^{2+} responses to IL-31 *ex vivo*.[4,12] Consistently, single-cell RNA sequencing (scRNA-seq) analysis showed that the *Il31ra* and *Osmr* genes are co-expressed in a subset of "non-peptidergic" neurons from DRGs.[4,13,14] Therefore, on the one hand, IL-31 receptor engagement in sensory neurons has been presumed to be responsible for the itch induction by this cytokine in some studies.[12,15] On the other hand, due to the relatively slow induction of itch after an IL-31 injection, it has also been proposed that IL-31 rather indirectly activates itch-transmitting nerves via other mediators.[16] In support of the latter idea, it was reported that IL-31-stimulated keratinocytes produce leukotriene B4 to induce itch.[17] However, direct *in vivo* evidence for the contribution of IL-31 receptor expressed by sensory neurons or keratinocytes to itch has not yet been provided.

IL-31 receptor engagement activates JAK1 and JAK2 of the JAK family, which in turn phosphorylate and activate signal transducer and activator of transcription (STAT) molecules STAT1, STAT3, and STAT5.[8] Among them, STAT3 was reported to be the main STAT activated after the *ex vivo* IL-31 stimulation of cultured mouse sensory neurons.[8,15] Nonetheless, it was suggested that STAT3 activation was dispensable for the itch induction by a single injection of IL-31.[15] Rather, activated STAT3 was suggested to be required for upregulation of the genes such as *Il31ra* and *Trpv1* in sensory neurons after the IL-31 injection, which would enhance itch induced by a second IL-31 injection.[15] However, these conclusions were based on the analysis of transgenic mice systemically expressing a dominant-negative STAT3 mutant,[15] and the impact of more efficient deletion of STAT3 activities specifically in sensory neurons is yet to be determined.

In the present study, we examined the contribution to itch of IL-31 receptor expressed in sensory neurons or keratinocytes by generating mice with cell-type-specific deletion of IL-31RA. Our data clearly indicate that IL-31RA expressed by sensory neurons but not by keratinocytes is required for the itch induction by IL-31. Unlike the previous study using the dominant-negative STAT3-expressing transgenic mice, our analysis using mice conditionally deficient in STAT3 indicated that sensory neuronal STAT3 is essential for IL-31-induced itch and also important for IL-31-independent itch associated with dermatitis.

RESULTS

Generation of mice with cell-type-specific IL-31RA deficiency

Both sensory neurons and keratinocytes have been proposed to contribute as IL-31-responsive cells during the itch induction by this cytokine, although the direct *in vivo* evidence is lacking.[12,15–17] In order to address this problem, we generated *Il31ra*-flox mice by introducing *loxP* sites flanking the exon 4, which contains the start codon (Figure S1A). The mice were bred with Nav1.8-Cre[18] or K5-Cre mice[19] to delete the *Il31ra* gene in C- and Aδ-fiber sensory neurons or keratinocytes. To evaluate the IL-31RA expression on sensory neurons, we performed immunofluorescence staining of DRG sections using the anti-mouse IL-31RA polyclonal antibody raised against Met28-Glu531. Strong staining signals for IL-31RA were largely colocalized with OSMR signals in a fraction of tdTomato$^+$ neurons in DRGs from Nav1.8-Cre Rosa26-CAG-floxStop-tdTomato (Nav1.8-Cre R26CAG-floxStop-tdTomato) mice (Figure 1A). In DRGs from Nav1.8-Cre R26CAG-floxStop-tdTomato *Il31ra*$^{fl/fl}$ mice, IL-31RA signals but not OSMR signals were greatly diminished on tdTomato$^+$ neurons (Figures 1A and S1B). We then analyzed IL-31RA expression in the skin by whole-mount immunofluorescence staining of the ear skin from Nav1.8-Cre R26CAG-floxStop-tdTomato mice. Consistent with the DRG staining results, IL-31RA$^+$ nerve fibers appeared to be a fraction of tdTomato$^+$ nerves (Figure 1B). As previously reported,[20,21] Nav1.8-tdTomato$^+$ nerves heavily innervated the epidermis. However, there were almost no IL-31RA$^+$ nerves found in the epidermis of normal mouse skin (Figures 1B and S1C). We found 86, 56, or 43 IL-31RA$^+$ nerve endings in 1.36 mm^2 (area) x 57–102 μm (thickness from the surface) of the ear skin from each of 3 mice. About one-half of the IL-31RA$^+$ nerve endings were located near the dermal-epidermal junction, while the other half were found within or near the nerve bundle in the dermis (Figures S1C and S1D). In the skin from Nav1.8-Cre R26CAG-flox-Stop-tdTomato *Il31ra*$^{fl/fl}$ mice, IL-31RA signals were not observed on Nav1.8-tdTomato$^+$ nerve fibers (Figure 1B). In contrast to the compelling IL-31RA signals in sensory neurons, IL-31RA signals were not clearly detected in the keratinocytes (Figure 1B). These results show that IL-31RA is expressed on sensory neurons that have nerve endings at the dermal-epidermal junction, and that IL-31RA expression is abolished in sensory neurons of Nav1.8-Cre *Il31ra*$^{fl/fl}$ mice. They also suggest that keratinocytes may not strongly express IL-31RA in the normal epidermis.

Characterization of IL-31-elicited scratching behavior

The previous studies reported that an intradermal or subcutaneous (s.c.) injection of IL-31 on the order of a microgram or more elicited significant scratching behavior in mice. However, these

Figure 1. IL-31-induced itch is dependent on IL-31RA expressed by sensory neurons

(A) Immunofluorescence images of DRG sections. Shown are representative images of 10 sections of 3 DRGs from 3 mice per group.

(B) Whole-mount confocal immunofluorescence images of the ear skin. The upper images are the vertical projection (34.5-μm projection depth). The lower images show horizontal views of the dashed rectangular regions in the vertical projection images. Shown are representative images of 3 ear skin samples from 3 mice per group.

(C–H) Numbers of scratching strokes after an s.c. injection of 2 μg IL-31 (C and D), 100 μg compound 48/80 (E and F), 400 μg chloroquine (G and H), or PBS (D, F, and H) at the nape. The graphs show mean and SEM for the indicated numbers of mice. *$p < 0.05$, **$p < 0.01$, ***$p < 0.001$, ****$p < 0.0001$. See STAR Methods for the information of the analyzed mice.

studies showed different time courses of scratching behavior using different doses of IL-31.[12,22] Therefore, we first characterized scratching behavior of IL-31RA-sufficient control mice elicited by 2 μg of IL-31 and found that it took longer than 10 min to elicit significant scratching bouts (Figure S1E). IL-31-elicited scratching became most intense around 25–55 min after the injection, and then it gradually decayed. In contrast, the injection of 100 μg compound 48/80, a known mast cell activator, more quickly elicited scratching as previously reported[23] (Figure S1E). The injection of 400 μg chloroquine, which was reported to act on the GPCR MRGPRA3 expressed mainly by different sensory neurons from those expressing IL-31 receptor,[13,20,24] also quickly elicited transient scratching (Figure S1E). Consistent with the previous reports,[22,23] a considerable number of IL-31-elicited scratching bouts were longer than 1.4 s, whereas most of compound 48/80- or chloroquine-elicited scratching bouts lasted less than 1.4 s (Figure S1F). However, we observed that IL-31 also induced many short-lasting bouts (Figure S1F) unlike the previous study.[22] IL-31 elicited scratching not only around the injection site but also in the distal skin areas (Figures S1G and S1H). In contrast, compound 48/80 and chloroquine elicited scratching primarily around the injection site (Figures S1G and S1H). Thus, an IL-31 injection induces itch relatively slowly, eliciting relatively long-lasting scratching bouts in both proximal and distal areas from the injection site.

Absence of sensory neuronal IL-31 receptor abolishes IL-31-induced itch

We then analyzed scratching behavior of the sensory neuron- or keratinocyte-selective IL-31RA-deficient mice injected with IL-31. We found that IL-31-elicited scratching was absent in Nav1.8-Cre *Il31ra*$^{fl/fl}$ mice (Figures 1C and 1D), while compound 48/80 or chloroquine elicited intact scratching behavior in these mice (Figures 1E–1H). In contrast, IL-31-elicited scratching behavior in K5-Cre *Il31ra*$^{fl/fl}$ mice was comparable to that of control mice (Figures 1C and 1D). Reverse transcription quantitative PCR (RT-qPCR) analysis revealed that *Il31ra* was efficiently deleted in DRGs from Nav1.8-Cre *Il31ra*$^{fl/fl}$ mice and in epidermal sheets but not in DRGs from K5-Cre *Il31ra*$^{fl/fl}$ mice (Figures S1I and S1J). These results indicate that IL-31RA expressed by sensory neurons but not by keratinocytes is essential for IL-31-induced itch.

Absence of sensory neuronal IL-31RA reduces itch associated with MC903-induced cutaneous inflammation

Next, we sought to investigate the contribution of IL-31RA expressed by sensory neurons or keratinocytes to chronic itch associated with dermatitis. As IL-31 has been reported to be produced by Th2 cells,[8] we employed an established model of cutaneous type 2 inflammation induced by a vitamin D3 analog MC903. Although a previous study did not find a significant contribution of the IL-31 signal to itch in this model,[4] other studies reported that mRNA of IL-31 was increased in the skin after the MC903 treatment.[25,26] As such, we sorted CD4$^+$ T cells as well as other CD45$^+$ cells (CD4-negative leukocytes) and CD45-negative cells (mainly non-leukocytes though possibly not completely excluding CD45-low basophils) from the ethanol vehicle-treated skin and MC903-treated skin (Figures 2A, S2A, and S2B) and analyzed the cytokine gene expression. Indeed, we found that *Il31* expression in CD4$^+$ T cells was increased after the MC903 treatment (Figure 2B). *Il31* expression was not increased in the other sorted cell populations (Figure 2B). We also examined *Il4* expression and found that it was increased most strikingly in CD4-negative leukocytes (Figure 2B). *Il4* expression tended to increase in CD4$^+$ T cells and CD45-negative cells, although the expression magnitude in these cells might be subtle compared to that in CD4-negative leukocytes (Figure 2B). The increased *Il4* expression in CD4-negative leukocytes is likely due to activated basophils, as reported previously.[27] Then, we analyzed pruritus development associated with MC903-induced dermatitis (Figure 2C) and found that Nav1.8-Cre *Il31ra*$^{fl/fl}$ mice showed less intense scratching behavior than control mice (Figure 2D). In contrast, scratching behavior of K5-Cre *Il31ra*$^{fl/fl}$ mice was not significantly different from that of control mice (Figure 2D). These results indicate that the IL-31 receptor of sensory neurons but not that of keratinocytes contributes to chronic itch of the dermatitis model.

STAT3 gene is dominantly expressed among STAT genes by C- and Aδ-fiber sensory neuron subsets

We then aimed to elucidate the role of the JAK-STAT pathway in IL-31-induced itch. To understand which STAT genes are expressed in the sensory neuronal subsets, we performed scRNA-seq analysis of tdTomato$^+$ DRG neurons from Nav1.8-Cre R26CAG-floxStop-tdTomato mice (Figures 3A and 3B). We clustered the scRNA-seq results by graph-based clustering into 5 populations as visualized in the t-distribution stochastic neighbor embedding (t-SNE) plot (Figure 3C): the "non-peptidergic" nociceptors (NP1, NP2, and NP3) that are thought to be involved in itch transmission based on their expression of the itch mediator receptor genes such as *Mrgprd* (NP1), *Mrgpra3* (NP2), and *Il31ra* (NP3); peptidergic nociceptors (PEP) involved in pain transmission and highly expressing the neuropeptide genes such as *Calca* and *Tac1*; and C-fiber low-threshold mechanoreceptors (Th) expressing the tyrosine hydroxylase gene (*Th*) (Figure 3D). The result is largely consistent with the previous study except that the peptidergic subsets were further divided into two subpopulations in the previous study.[13] Each subset expressed a set of signature genes that were reported in the previous study[13] (Figures 3D and S3A). Our data as well as the data of the previous study show that the *Stat3* gene was the most abundantly expressed among the STAT family genes in these neuronal subsets (Figures 3E and S3B). At the same time, our analysis detected that *Il31ra* and *Osmr* are co-expressed at relatively low magnitudes in a fraction of NP2 neurons (Figure 3F), which was not evident in the previous data[13] (Figure S3C).

STAT3 deficiency in sensory neurons reduces expression of IL-31 receptor and *Nppb* and abolishes IL-31-induced itch

The above results led us to examine the role for STAT3 in sensory neurons in IL-31-induced itch by generating Nav1.8-Cre *Stat3*$^{fl/fl}$ mice. Our analysis revealed that IL-31-elicited scratching behavior was virtually absent in Nav1.8-Cre *Stat3*$^{fl/fl}$ mice (Figures 4A and 4B), indicating that STAT3 in sensory neurons

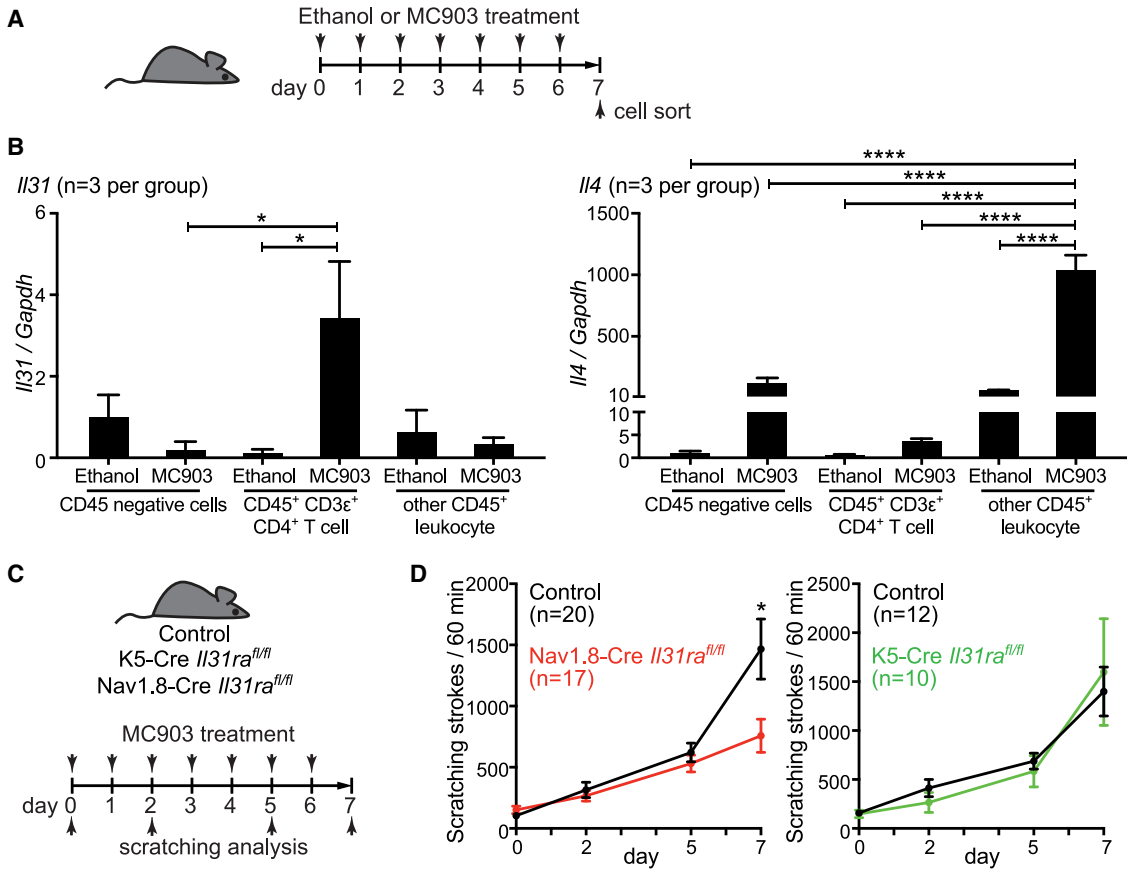

Figure 2. Absence of IL-31RA in sensory neurons reduces itch during MC903-induced cutaneous inflammation

(A) The time course of the topical ethanol or MC903 treatment to the ears for cell sorting.

(B) RT-qPCR analysis of the sorted cells from the ear skin treated with ethanol or MC903. *Gapdh*-normalized expression of *Il4* and *Il31* compared to that in CD45- negative cells from ethanol-treated skin is shown as mean and SEM for 3 independently sorted cell samples. *p < 0.05, ****p < 0.0001.

(C) The time course of the topical MC903 treatment for the scratching analysis.

(D) Numbers of scratching strokes per 60 min of MC903- or ethanol-treated mice with the indicated genotypes. The graphs show mean and SEM for the indicated numbers of mice per group. *p < 0.05. See STAR Methods for the information of the analyzed mice.

is required for IL-31-induced itch, in contrast to the result of the previous study using the dominant-negative STAT3 transgenic mice.[15] Scratching behavior elicited by compound 48/80, chloroquine, or N-methyl leukotriene C4 (mLTC4), a nonhydrolyzable form of leukotriene C4, which was reported to induce itch by acting on CysLTR2 expressed in NP3 neurons,[29–31] was intact in Nav1.8-Cre *Stat3*$^{fl/fl}$ mice (Figures 4C, 4D, and S4A). By immunofluorescence staining of DRG sections, we found that sensory neuronal expression of IL-31RA and OSMR was markedly diminished in Nav1.8-Cre *Stat3*$^{fl/fl}$ mice (Figures 4E and 4F). RNA-expression of *Il31ra* and *Osmr* was also reduced in sensory neurons of Nav1.8-Cre *Stat3*$^{fl/fl}$ mice (Figure S4B). As expected, *Stat3* expression was significantly reduced (Figure 4G), although the deletion efficiency might be lower than that of *Il31ra* in Nav1.8-Cre *Il31ra*$^{fl/fl}$ mice (Figure S1I). In addition, we observed a partial reduction in the expression of *Nppb* encoding the precursor of B-type natriuretic peptide in STAT3-deficient sensory neurons (Figure S4B). This peptide has been reported to be involved in transmission of itch including IL-31-induced itch.[32–34] Expression of *Sst* encoding somatostatin, another peptide hormone involved in itch transmission,[35] was not reduced in STAT3-deficient sensory neurons (Figure S4B). Consistently, the frequency of somatostatin-expressing DRG neurons was not decreased in Nav1.8-Cre *Stat3*$^{fl/fl}$ mice (Figures S4C and S4D). Expression of an NP1 neuron-selective gene *Mrgprd* was also intact in STAT3-deficient sensory neurons (Figure S4B). The frequencies of Nav1.8-tdTomato^{+} neurons expressing GFRα2 and GFRα1, which are encoded by *Gfra2* and *Gfra1* expressed in the NP1/Th subset and NP2 subset, respectively (Figure 3D), were comparable between control and Nav1.8-Cre *Stat3*$^{fl/fl}$ mice (Figures S4E–S4H). These results suggest that sensory neuronal STAT3 is important for constitutive expression of the IL-31 receptor genes, contributes to *Nppb* expression in sensory neurons, and is essential for IL-31-induced itch, though it may not be required for gross differentiation of non-peptidergic neurons.

Acute partial inhibition of STAT3 activation reduces IL-31-induced itch

Since the genetic deletion of STAT3 in sensory neurons impaired constitutive expression of IL-31 receptor, we sought

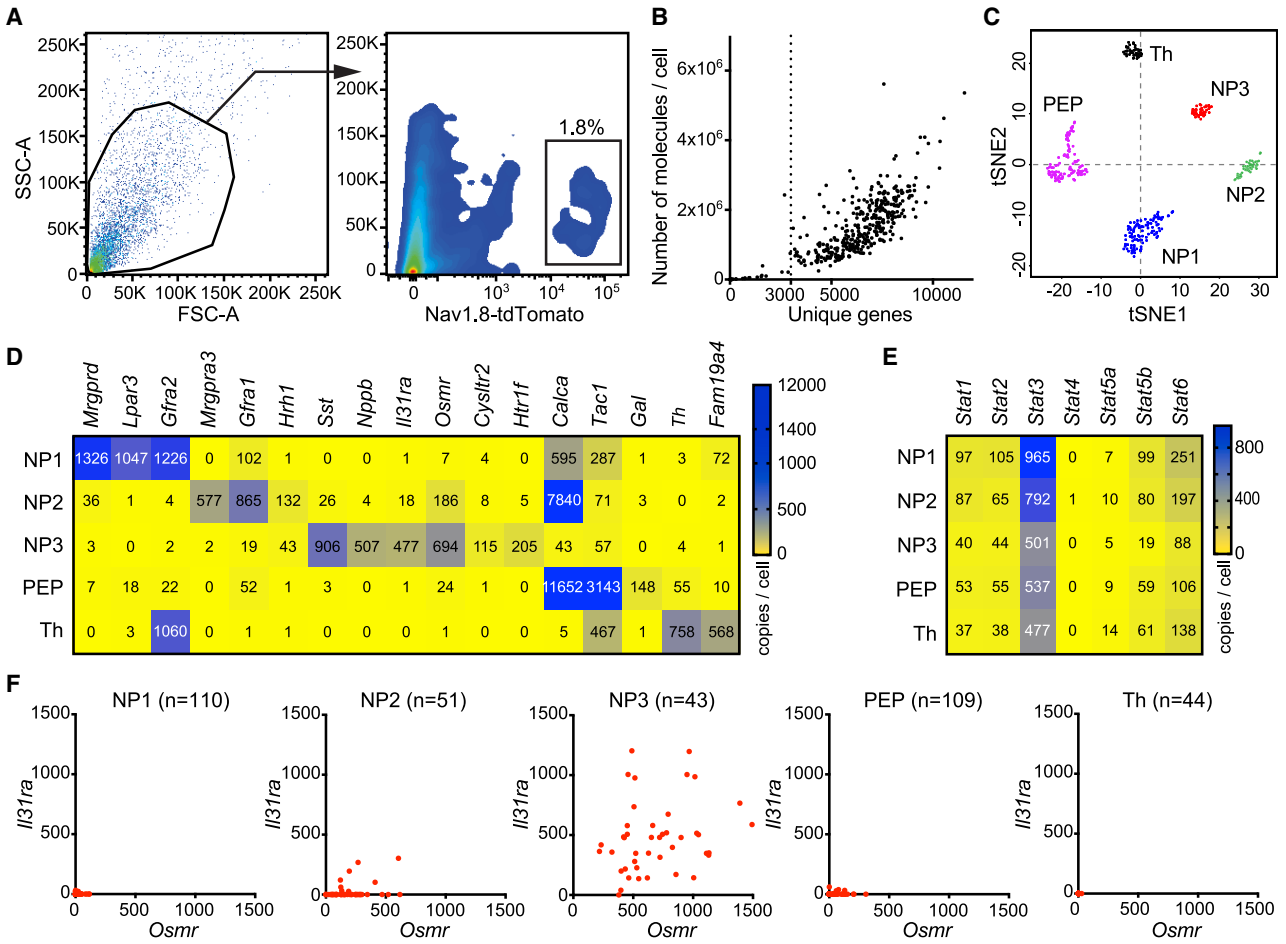

Figure 3. Expression of the STAT genes and IL-31 receptor genes by C- and Aδ-fiber sensory neuron subsets

(A) Representative flow cytometry plots showing the gating strategy to obtain tdTomato$^+$ cells from DRGs of Nav1.8-Cre R26CAG-floxStop-tdTomato mice for the scRNA-seq analysis.

(B) Numbers of unique genes and numbers of transcripts detected in individual Nav1.8-tdTomato$^+$ cells analyzed by scRNA-seq.

(C) The tSNE plot shows the neuronal subsets identified by unsupervised clustering analysis of 357 cells from 6 mice using the Seurat package.[28]

(D and E) The heatmaps show mean transcript numbers detected per cell of the subset-selective genes (D) and the *Stat* genes (E).

(F) Transcript numbers of *Il31ra* and *Osmr* plotted for each cell of the indicated neuronal subsets. See STAR Methods for the information of the analyzed mice.

to take a pharmacological approach to address the role for STAT3 activation downstream of IL-31 receptor in the itch induction. Thus, we tested the effect of the STAT3 antagonist S3I-201. We found that the treatment with S3I-201 at 10 mg/kg body weight 30 min prior to an IL-31 injection partially but significantly reduced IL-31-elicited scratching (Figures 4H–4J). In contrast, chloroquine-elicited scratching was not affected by the S3I-201 treatment (Figure 4K). The immunofluorescence analysis detected robust signals of Tyr705-phosphorylated STAT3 (pSTAT3) in nuclei of sensory neurons, especially IL-31RA-expressing neurons in the C2 DRGs at 15 min after an IL-31 injection in the nape skin (Figure 4L). The S3I-201 treatment partially but significantly reduced the nuclear pSTAT3 signals in sensory neurons of IL-31-injected mice (Figures 4L and 4M). These results suggest that STAT3 activation downstream of IL-31 receptor is involved in the itch induction.

Activated STAT3 is rapidly accumulated in nuclei of NP3 neurons and subsequently in nuclei of a fraction of NP2 neurons after IL-31 injection in skin

We then performed a time course analysis of nuclear pSTAT3 accumulation in sensory neurons following an s.c. injection of IL-31. We found increased staining signals of pSTAT3 in some nuclei of IL-31RA$^+$ neurons in the DRGs as early as 5 min after s.c. injecting IL-31 (Figures 5A and 5B). At 10 min after the injection, pSTAT3 staining signals were increased in the majority of IL-31RA$^+$ neurons in the DRGs (Figures 5A and 5B). At this time point, signals of pSTAT3 were detected also in nuclei of a small number of IL-31RA-negative or -low neurons (Figure 5A). At 15 min after the injection, signals of pSTAT3 were further increased in nuclei of IL-31RA$^+$ neurons and were also found in nuclei of a considerable number of IL-31RA-negative or -low neurons (Figures 5A and 5B). We speculated that the pSTAT3$^+$ IL-31RA-negative or -low neurons might be NP2 neurons, given

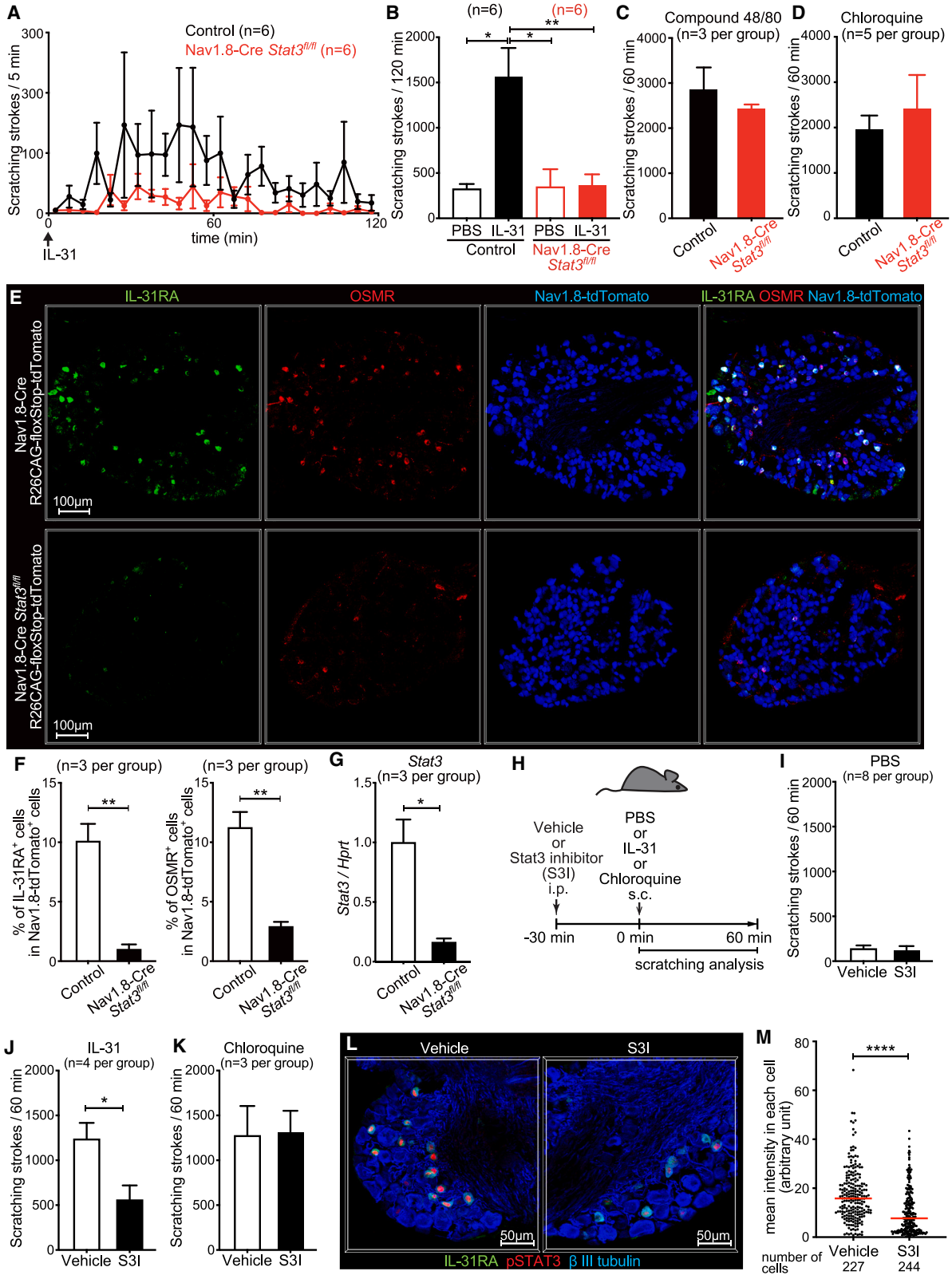

(legend on next page)

that a fraction of NP2 neurons express *Il31ra* together with *Osmr* at low levels (Figure 3F). To test this possibility, we stained DRG sections for GFRα1, Nav1.8-tdTomato, and pSTAT3 (Figure S5A). As a result, we found that a fraction of GFRα1$^+$ Nav1.8-tdTomato$^+$ NP2 neurons were pSTAT3$^+$ at 10 min and 15 min after the IL-31 injection (Figures 5C and S5A). In contrast, GFRα2$^+$ Nav1.8-tdTomato$^+$ NP1/Th neurons were mostly negative for pSTAT3 at these time points (Figures 5D and S5B). At 90 min after the injection, nuclear pSTAT3 signals in IL-31RA$^+$ NP3 neurons were largely sustained (Figures 5A and 5B). At this time point, nuclear pSTAT3 signals were detected in the majority of GFRα1$^+$ Nav1.8-tdTomato$^+$ NP2 neurons and also in a small number of GFRα2$^+$ Nav1.8-tdTomato$^+$ NP1/Th neurons (Figures 5C and 5D). By 180 min after the injection, nuclear pSTAT3 signals partially decayed in NP3 neurons and almost back to the steady-state level in NP2 and NP1 neurons (Figures 5A–5D). As expected, pSTAT3 staining signals were significantly diminished in DRGs of Nav1.8-Cre *Stat3$^{fl/fl}$* R26CAG-floxStop-tdTomato mice injected with IL-31 (Figures S5C and S5D). These results suggest that the accumulation of activated STAT3 in nuclei of NP3 neurons takes place in a similar time course with the itch induction after an IL-31 injection in the skin, and that NP2 neurons relatively slowly accumulate activated STAT3 in their nuclei after the IL-31 injection, possibly due to low expression of IL-31 receptor and/or by unknown mechanisms.

IL-31 enhances itch induced by various GPCR stimulations

It seemed likely that IL-31-transduced signals in NP3 and NP2 neurons could augment itch induced by other pruritogens. Therefore, we tested the effect of IL-31 pretreatment on itch induced by various GPCR stimulations to NP3 and NP2 neurons. The histamine receptor gene *Hrh1* is expressed in both NP2 and NP3 neurons[13,29] (Figure 3D). The previous study showed that scratching behavior elicited by a low dose of histamine was enhanced by co-injecting IL-4.[4] Because IL-31 induces intense itch by itself unlike IL-4, we injected a low dose of histamine (5 μg, see Figure S6A) 4 h after an IL-31 injection, by which time IL-31-elicited scratching counts dropped back to the baseline level (Figures 6A and 6B). As the result, we found that the IL-31 pretreatment markedly intensified the scratching behavior triggered by a low dose of histamine (Figures 6B and 6C). The IL-31 pretreatment also augmented scratching behavior induced by a suboptimal dose of mLTC4 (0.5 μg, see Figure S6B), although the enhancement was relatively modest (Figures S6C–S6E). We also sought to develop a chemogenetic method for *in vivo* NP3-selective GPCR stimulation. For this purpose, we generated *Il31ra*-T2A-Cre mice in which Cre was designed to be co-expressed with IL-31RA in cells that inherently express the *Il31ra* gene (Figure S6F), and we crossed them with Rosa26-CAG-FLEX-hM3Dq-mCherry (R26CAG-FLEX-hM3Dq) mice[36] (Figure 6D). In DRGs of the resultant *Il31ra*-T2A-Cre R26CAG-FLEX-hM3Dq mice, mCherry fused to the modified human M3 muscarinic receptor hM3Dq was detected almost exclusively in IL-31RA-expressing neurons (Figures 6E and S6G). Unexpectedly, clozapine-N-oxide (CNO), the artificial ligand for hM3Dq, by itself did not lead to significant scratching in *Il31ra*-T2A-Cre R26CAG-FLEX-hM3Dq mice when injected s.c. or intraperitoneally with CNO (Figures S6H and S6I). However, a CNO injection immediately elicited intense but transient scratching in IL-31-pre-treated *Il31ra*-T2A-Cre R26CAG-FLEX-hM3Dq mice but not in IL-31-pre-treated control mice (Figures 6F–6H). As a GPCR stimulation to NP2 neurons, we used chloroquine whose receptor was reported to be MRGPRA3 expressed in NP2 neurons.[24] Because the high chloroquine dose (400 μg) by itself elicited intense scratching (Figures 1G, 1H, S1E, 4D, 4K, and S6J), we used a lower dosage (40 μg) that elicited only mild scratching on its own (Figure S6J). However, an injection of the low dose of chloroquine immediately elicited intense scratching in IL-31-pre-treated mice (Figures 6I–6K). These results suggest that IL-31 receptor signaling in NP3 and NP2 neurons greatly amplifies itch induced by GPCR stimulation of these neurons.

STAT3 in sensory neurons is essential for pruritus of the atopic dermatitis model

Finally, we investigated whether the absence of sensory neuronal STAT3 might have a broader/more extensive effect on pruritus associated with dermatitis than the absence of IL-31 receptor signaling. Indeed, we found that scratching elicited by repetitive treatment with MC903 was diminished in Nav1.8-Cre *Stat3$^{fl/fl}$* mice (Figures 7A and 7B). In C1-C2 DRGs of MC903-treated control mice, pSTAT3 was found in nuclei of NP3 and NP2 neurons (Figures 7C–7H). In addition, activated STAT3 was also found in

Figure 4. Involvement of sensory neuronal STAT3 in expression of IL-31 receptor and downstream signaling for itch induction

(A–D) Numbers of scratching strokes after an s.c. injection of 2 μg IL-31 (A and B), PBS (B), 100 μg compound 48/80 (C), or 400 μg chloroquine (D) at the nape of control and Nav1.8-Cre *Stat3$^{fl/fl}$* mice.

(E) Immunofluorescence images of DRG sections. Shown are representative images of 10 sections of 3 DRGs from 3 mice per group.

(F) Percentages of IL-31RA$^+$ neurons and OSMR$^+$ neurons in Nav1.8-tdTomato$^+$ neurons in DRG sections from Nav1.8-Cre R26CAG-floxStop-tdTomato mice (control) and Nav1.8-Cre *Stat3$^{fl/fl}$* R26CAG-floxStop-tdTomato mice (Nav1.8-Cre *Stat3$^{fl/fl}$*).

(G) RT-qPCR analysis of *Stat3* expression in tdTomato$^+$ neurons sorted from the DRGs of Nav1.8-Cre R26CAG-floxStop-tdTomato mice (control) and Nav1.8-Cre *Stat3$^{fl/fl}$* R26CAG-floxStop-tdTomato mice (Nav1.8-Cre *Stat3$^{fl/fl}$*).

(H) Schematic showing the time course of vehicle or STAT3 inhibitor treatment and an injection with PBS, IL-31, or chloroquine for the scratching analysis.

(I–K) Numbers of scratching strokes after an s.c. injection of PBS (I), 2 μg IL-31 (J), or 400 μg chloroquine (K) at the nape of wild-type mice pre-treated with the vehicle or the STAT3 inhibitor S3I-201 (S3I). The graphs (A–D, F, G, and I–K) show mean and SEM for the indicated numbers of mice per group. *$p < 0.05$, **$p < 0.01$, ***$p < 0.001$.

(L) Immunofluorescence images of DRG sections from mice pre-treated with the vehicle or S3I and injected with IL-31. C2-C4 DRGs were harvested at 15 min after the IL-31 injection.

(M) Intensities of pSTAT3 staining signals in individual IL-31RA$^+$ neurons. The data were pooled from the indicated numbers of cells in 14 sections (vehicle) or 18 sections (S3I) of 3 DRGs from 3 mice per group. ****$p < 0.0001$. See STAR Methods for the information of the analyzed mice.

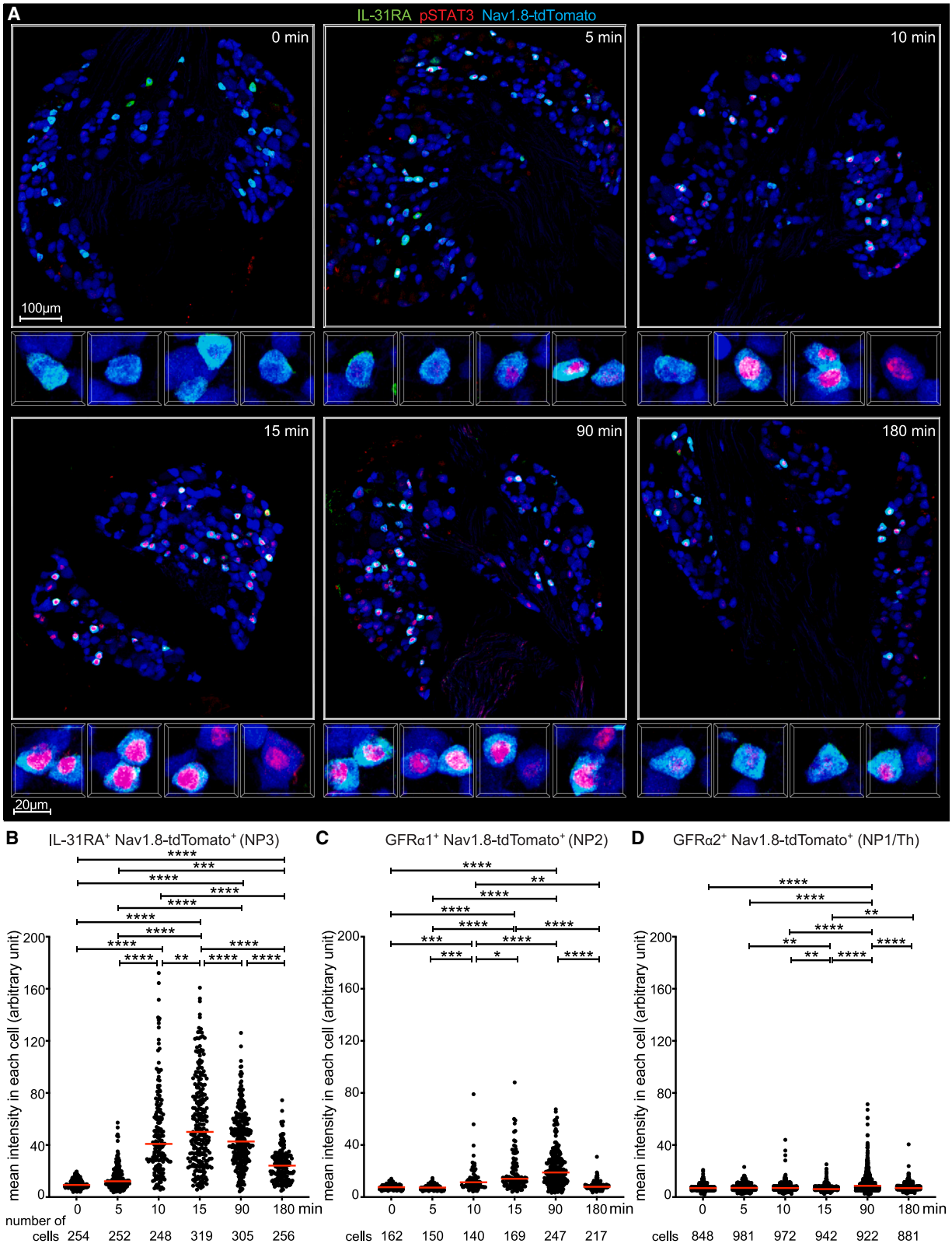

(legend on next page)

nuclei of NP1 and/or Th neurons (Figures 7I–7K). As expected, nuclear accumulation of activated STAT3 in sensory neurons was diminished in DRGs of MC903-treated Nav1.8-Cre *Stat3*$^{fl/fl}$ mice (Figures S7A and S7B). These results suggest that sensory neuronal STAT3 plays critical roles for inflammatory itch induced not only by IL-31 but also by other mediators.

DISCUSSION

The inhibition of type 2 cytokine signaling is becoming an increasingly promising strategy for the treatment against chronic itch diseases such as atopic dermatitis and prurigo nodularis. It is now acknowledged that type 2 cytokine signaling in sensory neurons plays an important role in the induction of pathological itch.[2] For example, IL-4/IL-13 receptor and JAK1 of sensory neurons were shown to be involved in itch of the MC903-induced dermatitis by the study using mice with sensory neuron-selective deficiency of these molecules.[4] It has been presumed that sensory neuron-expressed IL-31 receptor is also important for itch, although direct *in vivo* evidence was lacking.[2,7] In addition, IL-31 receptor signaling in keratinocytes was suggested to be involved in the itch induction.[7,16,17] Our study provides the direct evidence that IL-31 receptor of sensory neurons but not of keratinocyte is essential for the itch induction by IL-31 in the normal mouse skin and is involved in the itch induction during MC903-induced inflammation. Future studies will need to evaluate contributions of IL-31 receptor expressed by different cell types to the itch induction in different disease models. In humans, however, it will be difficult to directly evaluate them. It was reported that IL-31 receptor was upregulated in human keratinocytes after various stimulations or in the condition of atopic dermatitis.[37,38] It will be important to study how IL-31 receptor signaling in human keratinocytes may contribute to itch by analyzing their productions of itch mediators and barrier function.[11]

Our data clearly indicate that STAT3 expressed by sensory neurons is essential for IL-31-induced itch. This appears to be, at least partly, due to the effect of sensory neuronal STAT3 on the steady-state expression of IL-31 receptor and *Nppb.*[34] This is in contrast with the previous report that itch induced by a first injection of IL-31 was intact in the transgenic mice expressing the dominant-negative form of STAT3.[15] The reason for this seeming discrepancy is not clear at this moment. However, it is likely that the dominant-negative STAT3 incompletely inhibited the activity of wild-type STAT3 in sensory neurons of the transgenic mice. The remaining wild-type STAT3 activity in the transgenic mice might be sufficient for maintaining constitutive expression of the IL-31 receptor genes and *Nppb* but not for upregulating *Il31ra* and Trpv1 expression after an IL-31 stimulation.[15] *Il31ra* but not *Osmr* or *Nppb* is suggested to be a STAT3 target gene by the ChIP-X Enrichment Analysis (ChEA: https://maayanlab.cloud/Harmonizome/gene_set/STAT3/CHEA+Transcription+Factor+Targets) using the database of genome-wide analyses of the binding of transcription factors to DNA.[39] However, the other studies have suggested that *Osmr* and *Nppb* are STAT3 target genes.[40,41] Future studies should determine whether STAT3 is directly involved in and what other transcription factors contribute to expression of the IL-31 receptor genes and *Nppb* in sensory neurons. It will be also important to investigate what signals and receptors are engaged to activate STAT3 for expression of the IL-31 receptor during differentiation of NP3 neurons.

Because our pharmacological analyses suggest that the itch induction by IL-31 is dependent on the immediate STAT3 activity, it is likely that STAT3-dependent gene expression downstream of IL-31 receptor is involved in the itch-inducing signaling pathway. This possibility is consistent with the observed time course of nuclear translocation of activated STAT3 preceding the itch induction after the IL-31 injection. It will be important to identify STAT3-target genes that are upregulated in NP3 neurons and essential for IL-31-induced itch. Our study also indicates that IL-31 signaling enhanced itch induced by the various GPCR stimulations. It is possible that STAT3 activation and the subsequent gene expression mediate the enhancement of GPCR-induced itch by IL-31. Unfortunately, the STAT3 antagonist could not be used to test this possibility because the suppression effect of the antagonist on IL-31-induced itch did not last long enough. After identifying STAT3-target genes important for IL-31-induced itch, their involvement in the enhancement of GPCR-induced itch should also be tested.

The chemogenetic stimulation of Gq-signaling pathways in NP3 neurons did not induce evident itch by itself, though it rapidly induced itch when it followed the IL-31 stimulation. In contrast, mLTC4 could induce mild itch by itself, reportedly by inducing Gq signaling downstream of the CysLTR2 receptor in NP3 neurons.[30,31] However, cysteinyl leukotrienes can activate their receptors in other cells such as fibroblasts and innate lymphoid cells[42,43] and may drive those cells to produce additional signals to activate NP3 neurons. Thus, we propose that Gq signaling alone in NP3 neurons is not sufficient for the itch induction, and that additional signals such as cytokines are required to enable itch transmission by NP3 neurons. Future studies should investigate what the cytokine signal does to make NP3 neurons ready to transmit itch upon the GPCR stimulation. The potential roles for the cytokine signals in NP3 neurons to be examined include the facilitation of neuropeptide/neurotransmitter production, loading, and/or release.

We found that chronic itch of the MC903-induced dermatitis model was strongly suppressed when sensory neurons are deficient in STAT3. In mice that lacked IL-31RA in sensory neurons, scratching induced by the MC903 treatment was only partially reduced. These observations together indicate that sensory neuronal STAT3 plays an important role in both IL-31-dependent and -independent itch in inflammatory conditions. The previous study showed that scratching of MC903-treated mice was

Figure 5. IL-31 induced nuclear accumulation of activated STAT3 in NP3 and a fraction of NP2 neurons

(A) Immunofluorescence images of pSTAT3 and IL-31RA in DRG sections from Nav1.8-Cre R26CAG-floxStop-tdTomato mice. C2 DRGs were harvested at the indicated time after an s.c. injection of 2 μg IL-31 at the nape.

(B–D) Intensities of pSTAT3 signals in individual IL-31RA$^+$ Nav1.8-tdTomato$^+$ cells (B), GFRα1$^+$ Nav1.8-tdTomato$^+$ cells (C), and GFRα2$^+$ Nav1.8-tdTomato$^+$ cells (D) at the indicated time points after an IL-31 injection. The data were pooled from the indicated numbers of cells in 9 or 12 sections of 3 or 4 DRGs from 3 or 4 mice per time point. *p < 0.05, **p < 0.01, ***p < 0.001, ****p < 0.0001. See STAR Methods for the information of the analyzed mice.

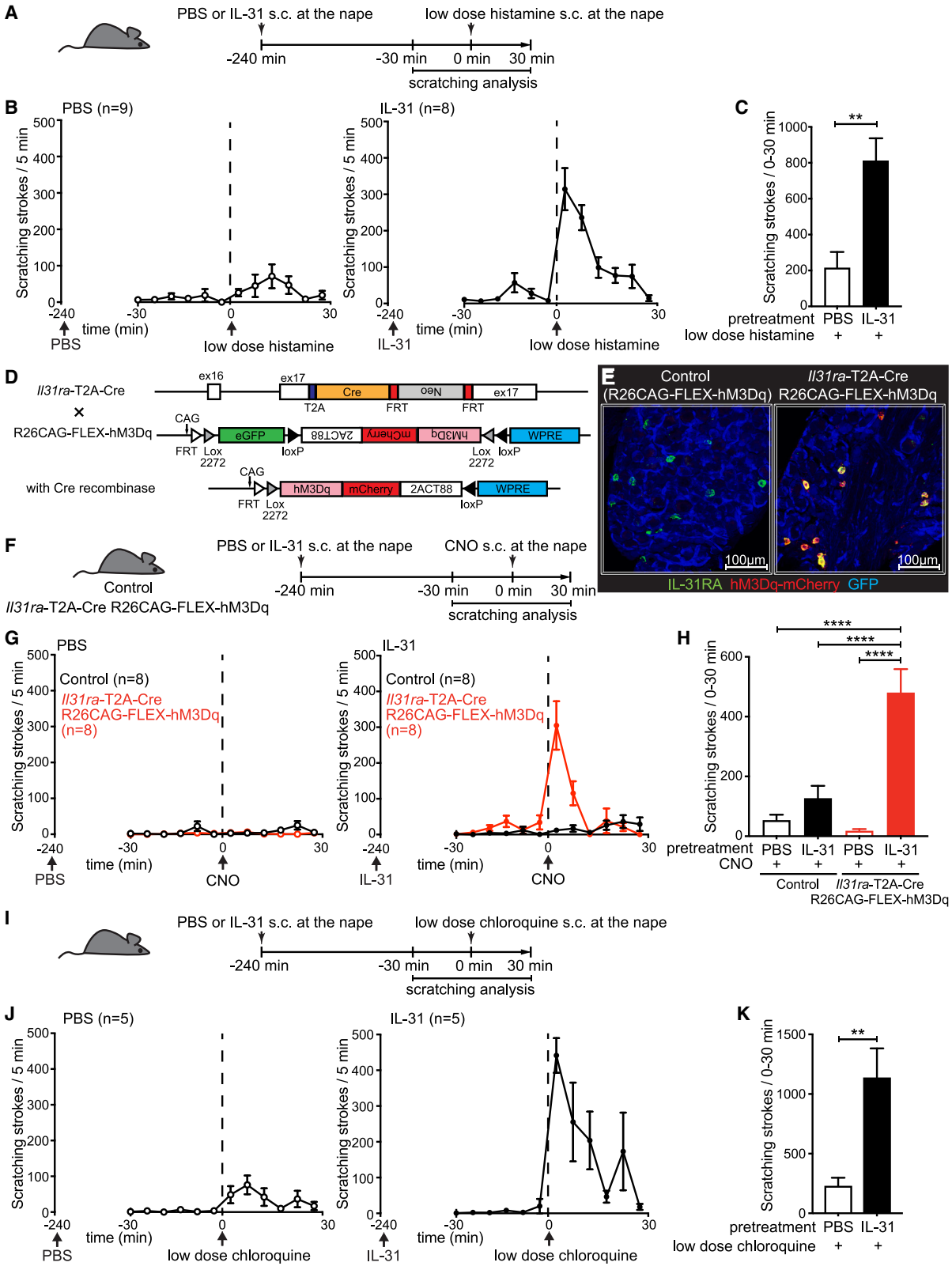

(legend on next page)

partially reduced by the absence of IL-4/13 receptor in sensory neurons.[4] It will be interesting to examine whether IL-4/13 induces STAT3-dependent signaling in sensory neurons, especially in NP1 and NP2 neurons. In addition, oncostatin M can potentiate itch of the MC903 model by acting on the OSMR/gp130 heterodimeric receptor of sensory neurons.[44] Our results show that sensory neuronal STAT3 deficiency not only impairs IL-31RA expression but also reduces OSMR expression. Furthermore, STAT3 is most likely involved in oncostatin M-induced signaling mechanisms. Therefore, it is highly possible that oncostatin M-dependent itch was also reduced in MC903-treated Nav1.8-Cre *Stat3*$^{fl/fl}$ mice.

Although itch of atopic dermatitis is most likely mediated by multiple pruritogens, the treatment with nemolizumab has been shown to effectively alleviate it.[9] Our study suggests that IL-31 receptor blockade not only inhibits IL-31-induced itch but also cancels the enhancement of GPCR-mediated itch by IL-31 signaling in multiple sensory neuron subsets. A recent scRNA-seq study of human DRGs has suggested that the majority of itch-transmitting human DRG neurons may express IL-31 receptor.[45] Therefore, it is possible that IL-31 can enhance a wide range of GPCR-mediated itch in humans, which may explain the broad effectiveness of nemolizumab against composite itch of atopic dermatitis. Finally, our work points out the importance of the development of inhibitors against human STAT3, which may have an even broader efficacy than the IL-31 receptor blockade but a lower risk of side effects than the inhibition of upstream JAK.[2]

Limitations of the study

Our results show an IL-31 injection can induce itch by itself. However, it is not clear whether the IL-31 dose (2 μg) used for injections in this study is relevant to actual disease conditions. The same caveat can be applied to our observation that a s.c. injection of IL-31 elicited scratching not only around the injection site but also in the distal skin areas. Future studies will need to measure IL-31 protein amounts in the skin of various pruritic dermatitis models to determine relevant dosages for the IL-31 injection. And then if a pathologically relevant dose of IL-31 elicits systemic scratching, the mechanism behind the phenomenon should be addressed.

Nav1.8-Cre mice were reported to express Cre in small-diameter neurons in DRGs from embryonic day 14.[18] Therefore, it is possible that differentiation of the sensory neurons was altered in Nav1.8-Cre *Stat3*$^{fl/fl}$ mice. However, these mice showed normal scratching responses to compound 48/80, chloroquine, and mLTC4. In addition, Nav1.8-Cre *Stat3*$^{fl/fl}$ mice had normal frequencies of DRG neurons expressing somatostatin (an NP3 marker), GFRα1 (an NP2 marker when combined with Nav1.8-tdTomato), and GFRα2 (an NP1/Th marker). Therefore, differentiation of non-peptidergic DRG neurons might not be grossly changed in Nav1.8-Cre *Stat3*$^{fl/fl}$ mice. Nonetheless, it is still possible that the STAT3 deficiency altered the sensory neuronal gene expression more broadly than just expression of IL-31 receptor and *Nppb*. Future studies should address this possibility by comprehensive analysis such as scRNA-seq of DRG neurons from Nav1.8-Cre *Stat3*$^{fl/fl}$ mice.

The study suggests the involvement of STAT3 activation downstream of IL-31 receptor in the itch induction mechanism only based on the pharmacological experiments using S3I-201, which only partially blocked IL-31-induced itch. Future studies should find and test other specific inhibitors that are more efficacious *in vivo* than S3I-201. In addition, methods to genetically interfere with STAT3 activation without impairing IL-31 receptor expression should be developed.

STAR★METHODS

Detailed methods are provided in the online version of this paper and include the following:

- KEY RESOURCES TABLE
- RESOURCE AVAILABILITY
  - Lead contact
  - Materials availability
  - Data and code availability
- EXPERIMENTAL MODEL AND SUBJECT DETAILS
  - Animals
- METHOD DETAILS
  - Immunofluorescence staining of DRG sections
  - Whole mount immunofluorescence staining of ear skin tissues
  - Confocal microscopy and image analysis
  - Bulk cell sorting from ear skin tissues
  - Bulk cell sorting from DRGs

Figure 6. IL-31 receptor signaling in sensory neurons enhances itch induced by various GPCR stimulations

(A) The time course of pretreatment with PBS or IL-31 and an injection with low-dose histamine for the scratching analysis.

(B) Numbers of scratching strokes before and after an s.c. injection of low-dose (5 μg) histamine into wild-type mice pre-treated with PBS (left graph) or 2 μg IL-31 (right graph) 4 h prior to the histamine injection.

(C) Numbers of scratching strokes in 30 min after the low-dose histamine injection in (A) and (B).

(D) Strategy for the generation of mice that allows chemogenetic stimulation of Gq signaling in NP3 neurons.

(E) Immunofluorescence images of DRGs from control (R26CAG-FLEX-hM3Dq) and *Il31ra*-T2A-Cre R26CAG-FLEX-hM3Dq mice. Shown are representative images of 17 sections of 3 DRGs from 3 mice per group.

(F) The time course of pretreatment with PBS or IL-31 and an injection with CNO for the scratching analysis.

(G) Numbers of scratching strokes before and after an s.c. injection of 22.5 μg CNO into control and *Il31ra*-T2A-Cre R26CAG-FLEX-hM3Dq mice pre-treated with PBS (left graph) or 2 μg IL-31 (right graph) 4 h prior to the CNO injection.

(H) Numbers of scratching strokes in 30 min after the CNO injection in (F) and (G).

(I) The time course of pretreatment with PBS or IL-31 and an injection with chloroquine for the scratching analysis.

(J) Numbers of scratching strokes before and after an s.c. injection of low-dose (40 μg) chloroquine into wild-type mice pre-treated with PBS (left graph) or IL-31 (right graph) 4 h prior to the chloroquine injection as shown in the diagram.

(K) Numbers of scratching strokes in 30 min after the low-dose chloroquine injection in (I) and (J). The graphs show mean and SEM for the indicated numbers of mice. $^{**}p < 0.01$, $^{****}p < 0.0001$. See STAR Methods for the information of the analyzed mice.

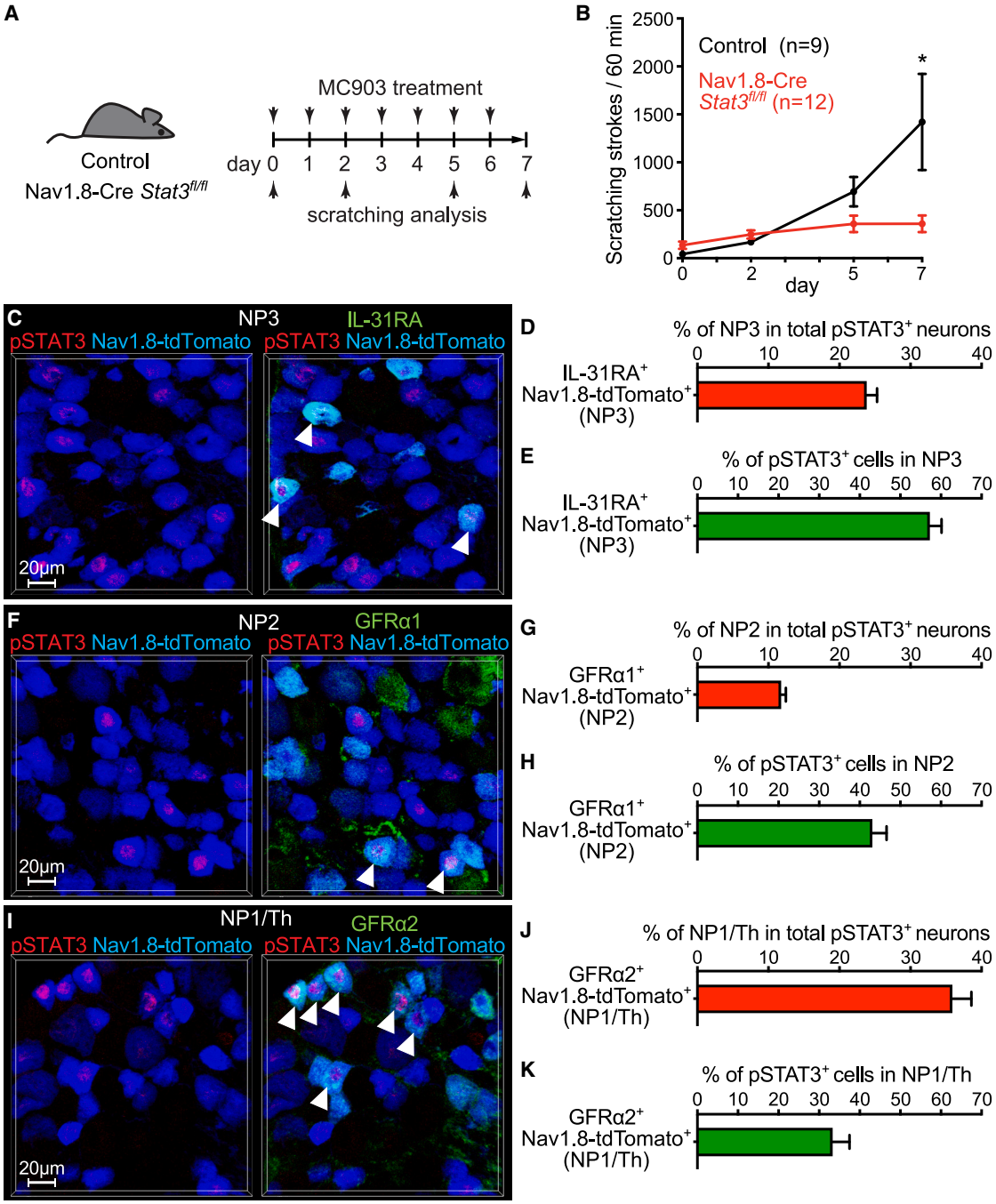

Figure 7. STAT3 in sensory neurons is important for pruritus associated with MC903-induced cutaneous inflammation

(A) The time course of the topical MC903 treatment to the ears.

(B) Numbers of scratching strokes of control and Nav1.8-Cre *Stat3*$^{fl/fl}$ mice treated with MC903. The graph shows mean and SEM for the indicated numbers of mice per group except for the day 2 time point (control: n = 7, Nav1.8-Cre *Stat3*$^{fl/fl}$: n = 8). *$p < 0.05$.

(C) Immunofluorescence images of pSTAT3 in DRG sections from MC903-treated Nav1.8-Cre R26CAG-floxStop-tdTomato mice on day 7. The section was co-stained for IL-31RA to identify NP3 neurons. The arrowheads indicate pSTAT3$^+$ NP3 neurons (see STAR Methods for the method to determine pSTAT3$^+$ neurons). The image without IL-31RA signals is shown in the left panel.

(D) Frequencies of pSTAT3$^+$ NP3 neurons in 956 pSTAT3$^+$ Nav1.8-tdTomato$^+$ neurons.

(E) Frequencies of pSTAT3$^+$ NP3 neurons in 399 NP3 neurons.

(F) Same as (C) except that the section was co-stained for GFRα1 to identify NP2 neurons.

(G) Frequencies of pSTAT3$^+$ NP2 neurons in 1,015 pSTAT3$^+$ Nav1.8-tdTomato$^+$ neurons.

(H) Frequencies of pSTAT3$^+$ NP2 neurons in 278 NP2 neurons.

(legend continued on next page)

- RT-qPCR
- *In vivo* treatments
- Scratching behavior analysis
- Single cell sorting of DRG neurons for scRNA-seq
- scRNA-seq
- Unsupervised clustering analysis using seurat package

● QUANTIFICATION AND STATISTICAL ANALYSIS

SUPPLEMENTAL INFORMATION

Supplemental information can be found online at https://doi.org/10.1016/j.celrep.2023.113433.

ACKNOWLEDGMENTS

We thank Kaori Fukuhara and Reiko Yamamoto for their technical assistance in library preparation and sequencing, Taisaku Ogawa, Junshi Yazaki, and Osamu Ohara for their technical support for the sequence analysis, Rumi Satoh for her help on cell sorting, Shizuo Akira for providing *Stat3*-flox mice, Junji Takeda for K5-Cre mice, and RIKEN IMS animal facility staffs for their assistance in generation and maintenance of the gene-targeted mice. We also are thankful for discussions with Masayuki Amagai, Hiroshi Kawasaki, Eiryo Kawakami, and Haruhiko Koseki. S.O. was supported by RIKEN Medical Sciences Innovation Hub Program (RIKEN MIH) and the Special Postdoctoral Researchers program at RIKEN. K.K. is supported by Japan Agency for Medical Research and Development (AMED) under CREST grant number JP23gm1210006. M.N. is supported by Platform Project for Supporting Drug Discovery and Life Science Research (Basis for Supporting Innovative Drug Discovery and Life Science Research (BINDS)) from AMED under grant number JP21am0101119. K.S. is supported by the Japan Society for the Promotion of Science (JSPS) KAKENHI grant 18H05411. T.O. was supported by AMED under grant number JP18ek0410033 and Japan Science and Technology Agency (JST) under CREST grant number JPMJCR17H1 and is supported by AMED under CREST grant number JP23gm1210006 and JST Moonshot R&D grant number JPMJMS2025.

AUTHOR CONTRIBUTIONS

S. Takahashi, S.O., and T.O designed the experiments. S. Takahashi, S.O., and S. Toshima performed the experiments and analyzed the data. S. Takahashi, S.O., N.T., H.I., M.K., M.N., and T.O. contributed to the generation of the genetically modified mice. J.J. and K.S. contributed to the scRNA-seq analysis. S. Takahashi, S.O., J.J., K.K., and T.O. wrote the manuscript.

DECLARATION OF INTERESTS

All authors declare that they have no relevant conflicts of interest.

Received: January 17, 2023
Revised: August 21, 2023
Accepted: October 30, 2023
Published: November 28, 2023

REFERENCES

1. Dong, X., and Dong, X. (2018). Peripheral and Central Mechanisms of Itch. Neuron *98*, 482–494. https://doi.org/10.1016/j.neuron.2018.03.023.
2. Wang, F., and Kim, B.S. (2020). Itch: A Paradigm of Neuroimmune Crosstalk. Immunity *52*, 753–766. https://doi.org/10.1016/j.immuni.2020.04.008.
3. Campion, M., Smith, L., Gatault, S., Métais, C., Buddenkotte, J., and Steinhoff, M. (2019). Interleukin-4 and interleukin-13 evoke scratching behaviour in mice. Exp. Dermatol. *28*, 1501–1504. https://doi.org/10.1111/exd.14034.
4. Oetjen, L.K., Mack, M.R., Feng, J., Whelan, T.M., Niu, H., Guo, C.J., Chen, S., Trier, A.M., Xu, A.Z., Tripathi, S.V., et al. (2017). Sensory Neurons Co-opt Classical Immune Signaling Pathways to Mediate Chronic Itch. Cell *171*, 217–228.e13. https://doi.org/10.1016/j.cell.2017.08.006.
5. Kamata, M., and Tada, Y. (2021). A Literature Review of Real-World Effectiveness and Safety of Dupilumab for Atopic Dermatitis. JID Innov. *1*, 100042. https://doi.org/10.1016/j.xjidi.2021.100042.
6. Simpson, E.L., Bieber, T., Guttman-Yassky, E., Beck, L.A., Blauvelt, A., Cork, M.J., Silverberg, J.I., Deleuran, M., Kataoka, Y., Lacour, J.P., et al. (2016). Two Phase 3 Trials of Dupilumab versus Placebo in Atopic Dermatitis. N. Engl. J. Med. *375*, 2335–2348. https://doi.org/10.1056/NEJMoa1610020.
7. Bağci, I.S., and Ruzicka, T. (2018). IL-31: A new key player in dermatology and beyond. J. Allergy Clin. Immunol. *141*, 858–866. https://doi.org/10.1016/j.jaci.2017.10.045.
8. Dillon, S.R., Sprecher, C., Hammond, A., Bilsborough, J., Rosenfeld-Franklin, M., Presnell, S.R., Haugen, H.S., Maurer, M., Harder, B., Johnston, J., et al. (2004). Interleukin 31, a cytokine produced by activated T cells, induces dermatitis in mice. Nat. Immunol. *5*, 752–760. https://doi.org/10.1038/ni1084.
9. Kabashima, K., Matsumura, T., Komazaki, H., and Kawashima, M.; Nemolizumab-JP01 Study Group (2020). Trial of Nemolizumab and Topical Agents for Atopic Dermatitis with Pruritus. N. Engl. J. Med. *383*, 141–150. https://doi.org/10.1056/NEJMoa1917006.
10. Ständer, S., Yosipovitch, G., Legat, F.J., Lacour, J.P., Paul, C., Narbutt, J., Bieber, T., Misery, L., Wollenberg, A., Reich, A., et al. (2020). Trial of Nemolizumab in Moderate-to-Severe Prurigo Nodularis. N. Engl. J. Med. *382*, 706–716. https://doi.org/10.1056/NEJMoa1908316.
11. Nakashima, C., Otsuka, A., and Kabashima, K. (2018). Interleukin-31 and interleukin-31 receptor: New therapeutic targets for atopic dermatitis. Exp. Dermatol. *27*, 327–331. https://doi.org/10.1111/exd.13533.
12. Cevikbas, F., Wang, X., Akiyama, T., Kempkes, C., Savinko, T., Antal, A., Kukova, G., Buhl, T., Ikoma, A., Buddenkotte, J., et al. (2014). A sensory neuron-expressed IL-31 receptor mediates T helper cell-dependent itch: Involvement of TRPV1 and TRPA1. J. Allergy Clin. Immunol. *133*, 448–460. https://doi.org/10.1016/j.jaci.2013.10.048.
13. Usoskin, D., Furlan, A., Islam, S., Abdo, H., Lönnerberg, P., Lou, D., Hjerling-Leffler, J., Haeggström, J., Kharchenko, O., Kharchenko, P.V., et al. (2015). Unbiased classification of sensory neuron types by large-scale single-cell RNA sequencing. Nat. Neurosci. *18*, 145–153. https://doi.org/10.1038/nn.3881.
14. Zeisel, A., Hochgerner, H., Lönnerberg, P., Johnsson, A., Memic, F., van der Zwan, J., Häring, M., Braun, E., Borm, L.E., La Manno, G., et al. (2018). Molecular Architecture of the Mouse Nervous System. Cell *174*, 999–1014.e22. https://doi.org/10.1016/j.cell.2018.06.021.
15. Xu, J., Zanvit, P., Hu, L., Tseng, P.Y., Liu, N., Wang, F., Liu, O., Zhang, D., Jin, W., Guo, N., et al. (2020). The Cytokine TGF-beta Induces Interleukin-31 Expression from Dermal Dendritic Cells to Activate Sensory Neurons and Stimulate Wound Itching. Immunity *53*, 371–383.e5. https://doi.org/10.1016/j.immuni.2020.06.023.
16. Hawro, T., Saluja, R., Weller, K., Altrichter, S., Metz, M., and Maurer, M. (2014). Interleukin-31 does not induce immediate itch in atopic dermatitis patients and healthy controls after skin challenge. Allergy *69*, 113–117. https://doi.org/10.1111/all.12316.

(I) Same as (C) except that the section was co-stained for GFRα2 to identify NP1/Th neurons.
(J) Frequencies of pSTAT3$^+$ NP1/Th neurons among 1,080 pSTAT3$^+$ Nav1.8-tdTomato$^+$ neurons.
(K) Frequencies of pSTAT3$^+$ NP1/Th neurons among 1,182 NP1/Th neurons. Data were from 14 sections for each staining condition of 4 DRGs from 4 mice and represented as mean and SEM for 4 mice (D, E, G, H, J, and K). See STAR Methods for the information of the analyzed mice.

17. Andoh, T., Harada, A., and Kuraishi, Y. (2017). Involvement of Leukotriene B4 Released from Keratinocytes in Itch-associated Response to Intradermal Interleukin-31 in Mice. Acta Derm. Venereol. *97*, 922–927. https://doi.org/10.2340/00015555-2697.

18. Stirling, L.C., Forlani, G., Baker, M.D., Wood, J.N., Matthews, E.A., Dickenson, A.H., and Nassar, M.A. (2005). Nociceptor-specific gene deletion using heterozygous NaV1.8-Cre recombinase mice. Pain *113*, 27–36. https://doi.org/10.1016/j.pain.2004.08.015.

19. Tarutani, M., Itami, S., Okabe, M., Ikawa, M., Tezuka, T., Yoshikawa, K., Kinoshita, T., and Takeda, J. (1997). Tissue-specific knockout of the mouse Pig-a gene reveals important roles for GPI-anchored proteins in skin development. Proc. Natl. Acad. Sci. USA *94*, 7400–7405. https://doi.org/10.1073/pnas.94.14.7400.

20. Han, L., Ma, C., Liu, Q., Weng, H.J., Cui, Y., Tang, Z., Kim, Y., Nie, H., Qu, L., Patel, K.N., et al. (2013). A subpopulation of nociceptors specifically linked to itch. Nat. Neurosci. *16*, 174–182. https://doi.org/10.1038/nn.3289.

21. Takahashi, S., Ishida, A., Kubo, A., Kawasaki, H., Ochiai, S., Nakayama, M., Koseki, H., Amagai, M., and Okada, T. (2019). Homeostatic pruning and activity of epidermal nerves are dysregulated in barrier-impaired skin during chronic itch development. Sci. Rep. *9*, 8625. https://doi.org/10.1038/s41598-019-44866-0.

22. Arai, I., Tsuji, M., Takeda, H., Akiyama, N., and Saito, S. (2013). A single dose of interleukin-31 (IL-31) causes continuous itch-associated scratching behaviour in mice. Exp. Dermatol. *22*, 669–671. https://doi.org/10.1111/exd.12222.

23. Inagaki, N., Igeta, K., Kim, J.F., Nagao, M., Shiraishi, N., Nakamura, N., and Nagai, H. (2002). Involvement of unique mechanisms in the induction of scratching behavior in BALB/c mice by compound 48/80. Eur. J. Pharmacol. *448*, 175–183. https://doi.org/10.1016/s0014-2999(02)01933-7.

24. Liu, Q., Tang, Z., Surdenikova, L., Kim, S., Patel, K.N., Kim, A., Ru, F., Guan, Y., Weng, H.J., Geng, Y., et al. (2009). Sensory neuron-specific GPCR Mrgprs are itch receptors mediating chloroquine-induced pruritus. Cell *139*, 1353–1365. https://doi.org/10.1016/j.cell.2009.11.034.

25. Li, M., Hener, P., Zhang, Z., Kato, S., Metzger, D., and Chambon, P. (2006). Topical vitamin D3 and low-calcemic analogs induce thymic stromal lymphopoietin in mouse keratinocytes and trigger an atopic dermatitis. Proc. Natl. Acad. Sci. USA *103*, 11736–11741. https://doi.org/10.1073/pnas.0604575103.

26. Hashimoto, T., Yokozeki, H., Karasuyama, H., and Satoh, T. (2023). IL-31-generating network in atopic dermatitis comprising macrophages, basophils, thymic stromal lymphopoietin, and periostin. J. Allergy Clin. Immunol. *151*, 737–746.e6. https://doi.org/10.1016/j.jaci.2022.11.009.

27. Pellefigues, C., Naidoo, K., Mehta, P., Schmidt, A.J., Jagot, F., Roussel, E., Cait, A., Yumnam, B., Chappell, S., Meijlink, K., et al. (2021). Basophils promote barrier dysfunction and resolution in the atopic skin. J. Allergy Clin. Immunol. *148*, 799–812.e10. https://doi.org/10.1016/j.jaci.2021.02.018.

28. Stuart, T., Butler, A., Hoffman, P., Hafemeister, C., Papalexi, E., Mauck, W.M., 3rd, Hao, Y., Stoeckius, M., Smibert, P., and Satija, R. (2019). Comprehensive Integration of Single-Cell Data. Cell *177*, 1888–1902.e21. https://doi.org/10.1016/j.cell.2019.05.031.

29. Solinski, H.J., Kriegbaum, M.C., Tseng, P.Y., Earnest, T.W., Gu, X., Barik, A., Chesler, A.T., and Hoon, M.A. (2019). Nppb Neurons Are Sensors of Mast Cell-Induced Itch. Cell Rep. *26*, 3561–3573.e4. https://doi.org/10.1016/j.celrep.2019.02.089.

30. Voisin, T., Perner, C., Messou, M.A., Shiers, S., Ualiyeva, S., Kanaoka, Y., Price, T.J., Sokol, C.L., Bankova, L.G., Austen, K.F., and Chiu, I.M. (2021). The CysLT2R receptor mediates leukotriene C4-driven acute and chronic itch. Proc. Natl. Acad. Sci. USA *118*, e2022087118. https://doi.org/10.1073/pnas.2022087118.

31. Wang, F., Trier, A.M., Li, F., Kim, S., Chen, Z., Chai, J.N., Mack, M.R., Morrison, S.A., Hamilton, J.D., Baek, J., et al. (2021). A basophil-neuronal axis promotes itch. Cell *184*, 422–440.e17. https://doi.org/10.1016/j.cell.2020.12.033.

32. Kiguchi, N., Sukhtankar, D.D., Ding, H., Tanaka, K.i., Kishioka, S., Peters, C.M., and Ko, M.C. (2016). Spinal Functions of B-Type Natriuretic Peptide, Gastrin-Releasing Peptide, and Their Cognate Receptors for Regulating Itch in Mice. J. Pharmacol. Exp. Ther. *356*, 596–603. https://doi.org/10.1124/jpet.115.229997.

33. Mishra, S.K., and Hoon, M.A. (2013). The cells and circuitry for itch responses in mice. Science *340*, 968–971. https://doi.org/10.1126/science.1233765.

34. Pitake, S., Ralph, P.C., DeBrecht, J., and Mishra, S.K. (2018). Atopic Dermatitis Linked Cytokine Interleukin-31 Induced Itch Mediated via a Neuropeptide Natriuretic Polypeptide B. Acta Derm. Venereol. *98*, 795–796. https://doi.org/10.2340/00015555-2977.

35. Huang, J., Polgár, E., Solinski, H.J., Mishra, S.K., Tseng, P.Y., Iwagaki, N., Boyle, K.A., Dickie, A.C., Kriegbaum, M.C., Wildner, H., et al. (2018). Circuit dissection of the role of somatostatin in itch and pain. Nat. Neurosci. *21*, 707–716. https://doi.org/10.1038/s41593-018-0119-z.

36. Sciolino, N.R., Plummer, N.W., Chen, Y.W., Alexander, G.M., Robertson, S.D., Dudek, S.M., McElligott, Z.A., and Jensen, P. (2016). Recombinase-Dependent Mouse Lines for Chemogenetic Activation of Genetically Defined Cell Types. Cell Rep. *15*, 2563–2573. https://doi.org/10.1016/j.celrep.2016.05.034.

37. Kato, A., Fujii, E., Watanabe, T., Takashima, Y., Matsushita, H., Furuhashi, T., and Morita, A. (2014). Distribution of IL-31 and its receptor expressing cells in skin of atopic dermatitis. J. Dermatol. Sci. *74*, 229–235. https://doi.org/10.1016/j.jdermsci.2014.02.009.

38. Kasraie, S., Niebuhr, M., Baumert, K., and Werfel, T. (2011). Functional effects of interleukin 31 in human primary keratinocytes. Allergy *66*, 845–852. https://doi.org/10.1111/j.1398-9995.2011.02545.x.

39. Lachmann, A., Xu, H., Krishnan, J., Berger, S.I., Mazloom, A.R., and Ma'ayan, A. (2010). ChEA: transcription factor regulation inferred from integrating genome-wide ChIP-X experiments. Bioinformatics *26*, 2438–2444. https://doi.org/10.1093/bioinformatics/btq466.

40. Ito, K., Noguchi, A., Uosaki, Y., Taga, T., Arakawa, H., and Takizawa, T. (2018). Gfap and Osmr regulation by BRG1 and STAT3 via interchromosomal gene clustering in astrocytes. Mol. Biol. Cell *29*, 209–219. https://doi.org/10.1091/mbc.E17-05-0271.

41. Unudurthi, S.D., Nassal, D., Greer-Short, A., Patel, N., Howard, T., Xu, X., Onal, B., Satroplus, T., Hong, D., Lane, C., et al. (2018). betaIV-Spectrin regulates STAT3 targeting to tune cardiac response to pressure overload. J. Clin. Invest. *128*, 5561–5572. https://doi.org/10.1172/JCI99245.

42. Oyoshi, M.K., He, R., Kanaoka, Y., ElKhal, A., Kawamoto, S., Lewis, C.N., Austen, K.F., and Geha, R.S. (2012). Eosinophil-derived leukotriene C4 signals via type 2 cysteinyl leukotriene receptor to promote skin fibrosis in a mouse model of atopic dermatitis. Proc. Natl. Acad. Sci. USA *109*, 4992–4997. https://doi.org/10.1073/pnas.1203127109.

43. Salimi, M., Stöger, L., Liu, W., Go, S., Pavord, I., Klenerman, P., Ogg, G., and Xue, L. (2017). Cysteinyl leukotriene E4 activates human group 2 innate lymphoid cells and enhances the effect of prostaglandin D2 and epithelial cytokines. J. Allergy Clin. Immunol. *140*, 1090–1100.e11. https://doi.org/10.1016/j.jaci.2016.12.958.

44. Tseng, P.Y., and Hoon, M.A. (2021). Oncostatin M can sensitize sensory neurons in inflammatory pruritus. Sci. Transl. Med. *13*, eabe3037. https://doi.org/10.1126/scitranslmed.abe3037.

45. Nguyen, M.Q., von Buchholtz, L.J., Reker, A.N., Ryba, N.J., and Davidson, S. (2021). Single-nucleus transcriptomic analysis of human dorsal root ganglion neurons. Elife *10*, e71752. https://doi.org/10.7554/eLife.71752.

46. Satija, R., Farrell, J.A., Gennert, D., Schier, A.F., and Regev, A. (2015). Spatial reconstruction of single-cell gene expression data. Nat. Biotechnol. *33*, 495–502. https://doi.org/10.1038/nbt.3192.

47. Madisen, L., Zwingman, T.A., Sunkin, S.M., Oh, S.W., Zariwala, H.A., Gu, H., Ng, L.L., Palmiter, R.D., Hawrylycz, M.J., Jones, A.R., et al. (2010). A

robust and high-throughput Cre reporting and characterization system for the whole mouse brain. Nat. Neurosci. *13*, 133–140. https://doi.org/10.1038/nn.2467.

48. Rodríguez, C.I., Buchholz, F., Galloway, J., Sequerra, R., Kasper, J., Ayala, R., Stewart, A.F., and Dymecki, S.M. (2000). High-efficiency deleter mice show that FLPe is an alternative to Cre-loxP. Nat. Genet. *25*, 139–140. https://doi.org/10.1038/75973.

49. Takeda, K., Kaisho, T., Yoshida, N., Takeda, J., Kishimoto, T., and Akira, S. (1998). Stat3 activation is responsible for IL-6-dependent T cell proliferation through preventing apoptosis: generation and characterization of T cell-specific Stat3-deficient mice. J. Immunol. *161*, 4652–4660.

50. Matsui, T., Kadono-Maekubo, N., Suzuki, Y., Furuichi, Y., Shiraga, K., Sasaki, H., Ishida, A., Takahashi, S., Okada, T., Toyooka, K., et al. (2021). A unique mode of keratinocyte death requires intracellular acidification. Proc. Natl. Acad. Sci. USA *118*, e2020722118. https://doi.org/10.1073/pnas.2020722118.

51. Shiroguchi, K., Jia, T.Z., Sims, P.A., and Xie, X.S. (2012). Digital RNA sequencing minimizes sequence-dependent bias and amplification noise with optimized single-molecule barcodes. Proc. Natl. Acad. Sci. USA *109*, 1347–1352. https://doi.org/10.1073/pnas.1118018109.

52. Ogawa, T., Kryukov, K., Imanishi, T., and Shiroguchi, K. (2017). The efficacy and further functional advantages of random-base molecular barcodes for absolute and digital quantification of nucleic acid molecules. Sci. Rep. *7*, 13576. https://doi.org/10.1038/s41598-017-13529-3.

53. Jin, J., Ogawa, T., Hojo, N., Kryukov, K., Shimizu, K., Ikawa, T., Imanishi, T., Okazaki, T., and Shiroguchi, K. (2023). Robotic data acquisition with deep learning enables cell image-based prediction of transcriptomic phenotypes. Proc. Natl. Acad. Sci. USA *120*, e2210283120. https://doi.org/10.1073/pnas.2210283120.

54. Dobin, A., Davis, C.A., Schlesinger, F., Drenkow, J., Zaleski, C., Jha, S., Batut, P., Chaisson, M., and Gingeras, T.R. (2013). STAR: ultrafast universal RNA-seq aligner. Bioinformatics *29*, 15–21. https://doi.org/10.1093/bioinformatics/bts635.

STAR★METHODS

KEY RESOURCES TABLE

REAGENT or RESOURCE	SOURCE	IDENTIFIER
Antibodies		
Mouse IL-31RA Antibody	R and D Systems	Cat# AF2107, RRID:AB_2124016
Rat GFR alpha-1/GDNF R alpha-1 Antibody	R and D Systems	Cat# AF560, RRID:AB_2110307
Human/Mouse GFR alpha-2/GDNF R alpha-2 Antibody	R and D Systems	Cat# AF429, RRID:AB_2294621
Anti-Mouse OSMR	MBL	Cat# D059-3, RRID:AB_592401
Anti-beta III Tubulin antibody (2G10)	Abcam	Cat# ab78078, RRID:AB_2256751
Phospho-Stat3 (Tyr705) (D3A7) XP Rabbit mAb	Cell Signaling Technology	Cat# 9145, RRID:AB_2491009
Anti-RFP pAb	MBL	Cat# PM005, RRID:AB_591279
Donkey anti-Goat IgG (H + L) Cross-Adsorbed Secondary Antibody, Alexa Fluor™ 488	Thermo Fisher Scientific	Cat# A-11055, RRID:AB_2534102
Donkey anti-Goat IgG (H + L) Cross-Adsorbed Secondary Antibody, Alexa Fluor™ 555	Thermo Fisher Scientific	Cat# A-21432, RRID:AB_2535853
Donkey anti-Goat IgG (H + L) Cross-Adsorbed Secondary Antibody, Alexa Fluor™ 647	Thermo Fisher Scientific	Cat# A-21447, RRID:AB_2535864
Donkey anti-Rat IgG (H + L) Highly Cross-Adsorbed Secondary Antibody, Alexa Fluor™ 488	Thermo Fisher Scientific	Cat# A-21208, RRID:AB_2535794
Rat monoclonal [SB84a] Anti-Mouse IgG2a heavy chain (Alexa Fluor® 488)	Abcam	Cat# ab172324
Donkey anti-Rabbit IgG (H + L) Highly Cross-Adsorbed Secondary Antibody, Alexa Fluor™ 488	Thermo Fisher Scientific	Cat# A-21206, RRID:AB_2535792
Donkey anti-Rabbit IgG (H + L) Highly Cross-Adsorbed Secondary Antibody, Alexa Fluor™ 647	Thermo Fisher Scientific	Cat# A-31573, RRID:AB_2536183
Rat Anti-CD16/CD32 Monoclonal Antibody, Unconjugated, Clone 2.4G2	BD Biosciences	Cat# 553141, RRID:AB_394656
PE Rat Anti-Mouse CD3 Molecular Complex (17A2)	BD Biosciences	Cat# 555275, RRID:AB_395699
APC anti-mouse CD4 (GK1.5)	BioLegend	Cat# 100412, RRID:AB_312697
APC/Cyanine7 anti-mouse CD45.2 (104)	BioLegend	Cat# 109824, RRID:AB_830789
Chemicals, peptides, and recombinant proteins		
Mouse Interleukin IL-31 Recombinant Protein	ROCKLAND	Car# 010-001-v66-0100
PBS(−)	Fujifilm Wako Chemicals	Cat# 166-23555
D-MEM (High Glucose) with L-Glutamine and Phenol Red	Fujifilm Wako Chemicals	Cat# 044-29765
BSA	Fujifilm Wako Chemicals	Cat# 018-15154
Triton X-100	Nacalai Tesque Inc.	Cat# 12968-35
Normal Donkey Serum	Jackson ImmunoResearch	Cat# 017-000-121, RRID:AB_2337258
Normal Rat Serum	Jackson ImmunoResearch	Cat# 012-000-120, RRID:AB_2337141
2-Mercaptoethanol	Fujifilm Wako Chemicals	Cat# 21438-82
Liberase TL Research Grade	Roche	Cat# 5401020001
Dispase II	Roche	Cat# 4942078001
papain	Sigma-Aldrich	Cat# P4762
DNase I	Roche	Cat# 11284932001
2-Mercaptoethanol	Fujifilm Wako Chemicals	Cat# 21438-82

(*Continued on next page*)

Continued

REAGENT or RESOURCE	SOURCE	IDENTIFIER
Cellstain DAPI Solution	Dojindo	Cat# D523
LIVE/DEAD™ Fixable Aqua Dead Cell Stain Kit	Thermo Fisher Scientific	Cat# L34957
Glycogen Solution	GMB	Cat# GM14
DEPC treated-Water	Nacalai Tesque Inc.	Cat# 36415-54
High-Capacity cDNA Reverse Transcription Kit	Applied Biosystems	Cat# 4374966
SYBR™ Green PCR Master Mix	Applied Biosystems	Cat# 4309155
MC903 (Calcipotriol)	TOCRIS	Cat# 2700
Compound 48/80	Sigma-Aldrich	Cat# C2313
Chloroquine diphosphate salt	Sigma-Aldrich	Cat# C6628
Histamine	Sigma-Aldrich	Cat# H7125
Clozapine N-oxide	Cayman Chemical	Cat# 16882
N-methyl Leukotriene C4	Cayman Chemical	Cat# 13390
S3I-201	Sigma-Aldrich	Cat# SML0330
Corn oil	Sigma-Aldrich	Cat# C8267
SingleCellProtect	Avidin Biotechnology	Cat# SCP-250
Fluorescence Mounting Medium	Dako	Cat# S3023
Tissue-Tek O.C.T Compound	Sakura Finetek	Cat# 45833
Deposited data		
scRNA-seq data	This paper	GEO: GSE218900
Experimental models: Organisms/strains		
Mouse: B6.129-Scn10a$^{tm2(cre)Jwo}$/H	Stirling et al., 2005	RRID:MGI:5496056
Mouse: B6.Cg-Gt(ROSA) 26Sor$^{tm14(CAG-tdTomato)Hze}$/J	The Jackson Laboratory	RRID:IMSR_JAX:007914
Mouse: B6.Cg-Gt(ROSA) 26Sor$^{tm3.2(CAG-EGFP,-CHRM3*/mCherry/Htr2a)Pjen}$/J	The Jackson Laboratory	RRID:IMSR_JAX:026942
Mouse: B6; SJL-Tg(ACTFLPe)9205Dym/J	The Jackson Laboratory	RRID:IMSR_JAX:003800
Mouse: Stat3-flox	Takeda et al., 1998	N/A
Mouse: K5-Cre	Tarutani et al., 1997	N/A
Mouse: Il31ra-flox	This paper	N/A
Mouse: Il31ra-T2A-Cre	This paper	N/A
Oligonucleotides		
ES screening primers and genotyping primers and RT-qPCR primers, see Table S1	This paper	N/A
Software and algorithms		
Flowjo	FlowJo, LLC	https://www.flowjo.com/solutions/flowjo
GraphPad Prism v9	GraphPad Software	https://www.graphpad.com/
Imaris 10.0.0	Bitplane	https://imaris.oxinst.com/
Seurat (v2.3.4) R package	Satija et al.[46] https://doi.org/10.1038/nbt.3192	https://satijalab.org/seurat/articles/install.html
Other		
PLATINUM PRO-coated glass slide	Matsunami Glass	Cat# PRO-01

RESOURCE AVAILABILITY

Lead contact

Further information and requests for resources and reagents should be directed to and will be fulfilled by the lead contact, Takaharu Okada (takaharu.okada@riken.jp).

Materials availability

The *Il31ra*-flox strain and *Il31ra*-T2A-Cre strain developed in this study will be deposited with RIKEN BioResource Center and made available for academic research.

Data and code availability

- All sequencing datasets have been deposited in the Genome Expression Omnibus database (GEO: GSE218900).
- This paper does not report original code.
- Any additional information required to reanalyze the data reported in this paper is available from the lead contact upon request.

EXPERIMENTAL MODEL AND SUBJECT DETAILS

Animals

C57BL/6J were purchased from CLEA Japan. Nav1.8-Cre mice[18] (EMMA ID: 04582) were obtained from Medical Research Council. R26CAG-floxStop-tdTomato mice[47] (Stock No: 007914) were obtained from the Jackson laboratory. Rosa26-CAG-FRT-Stop-FRT-FLEX-hM3Dq-mCherry mice[36] (Stock No:026942) and ACTB-FLPe mice[48] (Stock No:003800) were also obtained from Jackson, and intercrossed to obtain R26CAG-FLEX-hM3Dq mice. *Stat3*-flox mice were obtained from Dr. Shizuo Akira.[49] K5-Cre mice were obtained from Dr. Junji Takeda.[19] To generate *Il31ra*-flox mice and *Il31ra*-T2A-Cre mice, the targeting vector was constructed as shown in Figures S1A and S6F, respectively. C57BL/6J × C57BL/6N hybrid ES clones that underwent the desired homologous recombination (see Figures S1A and S6F) were selected and injected into BALB/c blastcysts. The ES screening primer pairs for *Il31ra*-flox mice were (i) 5′-gggtgtgatcttgtagctgcc-3′ and (ii) 5′- gtcaagaaggcgatagaaggcg-3′, and (iii) 5′-cagtcatagccgaatagcctc-3′ and (iv) 5′-gttaaattaaacaaagtctcctgtcga-3’ (Figure S1A). The genotyping primers for *Il31ra*-flox mice were (v) 5′-ccaatgtcaaaagcttcatcctacc-3′, (vi) 5′-ggcaagcaacaagctctgaacag-3′, and (vii) 5′-gctctcagacgtcgcttggtcggt-3’ (Figure S1A). The ES screening primer pairs for *Il31ra*-T2A-Cre mice were (i) 5′-tgtcctgactgctcttgccag-3′ and (ii) 5′-gaggctattcggctatgactg-3′, and (iii) 5′-cgccttctatcgccttcttgac-3′ and (iv) 5′-gaaggtttctggacatccgtc-3’ (Figure S6F). The genotyping primers for *Il31ra*-T2A-Cre mice were (v) 5′-gacaaccaggaatttcttgtgc-3′, (vi) 5′-cctgtgtgctctcacagaggccccttg-3′, and (vii) 5′-ggcagtaaaaactatccagcaacattt-3’ (Figure S6F). Chimeric male mice were mated with C57BL/6J female mice for germline transmission of the targeted *Il31ra* alleles. To generate *Il31ra*-T2A-Cre R26CAG-FLEX-hM3Dq mice, male *Il31ra*-T2A-Cre mice needed to be crossed with female R26CAG-FLEX-hM3Dq mice. Crossing female *Il31ra*-T2A-Cre mice with male mice with Cre-sensitive alleles caused germline recombination in the Cre-sensitive alleles of their offspring. Crossing mice that already had both the *Il31ra*-T2A-Cre and Cre-sensitive alleles, too, caused germline recombination in the Cre-sensitive alleles of their offspring. The mice were backcrossed to C57BL/6J mice for 5 to 6 generations and maintained in the specific pathogen-free condition at the RIKEN Yokohama Campus. Littermates or age-matched mice (see each figure legend for details) were used within each experiment. All experimental procedures were approved by the RIKEN Animal Experiment Committee, and all experiments were performed in according to the institutional guidelines.

The information of the mice used in each figure is as below.

Figures 1 and S1: The mice backcrossed to C57BL/6J mice for 5 generations were analyzed at the age of 7–11 week (Figures 1A–1H and S1B–S1D) and 9–16 weeks (Figures S1I and S1J). In Figures 1C–1H, S1I, and S1J, the control mice had the genotypes of *Il31ra*$^{fl/+}$, *Il31ra*$^{fl/fl}$, Nav1.8-Cre *Il31ra*$^{fl/+}$, or K5-Cre *Il31ra*$^{fl/+}$, and were littermates of the Nav1.8-Cre *Il31ra*$^{fl/fl}$ or K5-Cre *Il31ra*$^{fl/fl}$ mice. In Figures S1C–S1H, female C57BL/6J mice at 8–9 weeks of age were analyzed.

Figures 2 and S2: The mice backcrossed to C57BL/6J mice for 5 generations were analyzed at the age of 8–9 weeks (Figures 2B, S2A, and S2B) and 7–15 weeks (Figure 2D). In Figures 2B, S2A and S2B, mice with the genotypes of *Il31ra*$^{fl/+}$, *Il31ra*$^{fl/fl}$, Nav1.8-Cre *Il31ra*$^{fl/+}$, and K5-Cre *Il31ra*$^{fl/+}$ were analyzed at the age of 8–9 weeks. In Figure 2D, the control mice had the genotypes of *Il31ra*$^{fl/+}$, *Il31ra*$^{fl/fl}$, Nav1.8-Cre *Il31ra*$^{fl/+}$, or K5-Cre *Il31ra*$^{fl/+}$, and were littermates of the Nav1.8-Cre *Il31ra*$^{fl/fl}$ or K5-Cre *Il31ra*$^{fl/fl}$ mice.

Figure 3: The mice backcrossed to C57BL/6J mice for 5 generations were analyzed at the age of 9–12 weeks.

Figures 4 and S4: The mice backcrossed to C57BL/6J mice for 5 generations were analyzed at the age of 6–12 weeks (Figures 4A–4D), 8–13 weeks (Figures 4E–4G and S4B–S4H), and 8–16 weeks (Figure S4A). In Figures 4A–4D and S4A, the control mice had the genotypes of *Stat3*$^{fl/fl}$ or Nav1.8-Cre *Stat3*$^{fl/+}$, and were littermates of the Nav1.8-Cre *Stat3*$^{fl/fl}$ mice. In Figures 4E–4G and S4B–S4H, the control Nav1.8-Cre R26CAG-floxStop-tdTomato mice were littermates of the Nav1.8-Cre *Stat3*$^{fl/fl}$ R26CAG-floxStop-tdTomato mice. In Figures 4I–4M, 8-10-week-old male and female C57BL/6J mice were analyzed.

Figures 5 and S5: The mice backcrossed to C57BL/6J mice for 5 generations were analyzed at the age of 7–13 weeks (Figures 5A–5D, S5A and S5B) and 8–13 weeks (Figures S5C and S5D). In Figures S5C and S5D, the control Nav1.8-Cre R26CAG-floxStop-tdTomato mice and Nav1.8-Cre *Stat3*$^{fl/fl}$ R26CAG-floxStop-tdTomato mice were not littermates but were from the same colonies.

Figures 6 and S6: In Figures 6B and 6C, the wild-type mice from the Nav1.8-Cre and *Il31ra*-T2A-Cre colonies backcrossed to C57BL/6J mice for 5 and 6 generations, respectively, were analyzed at the age of 9–12 weeks. In Figures S6A, S6B, S6D, and S6E, the wild-type mice from the *Il31ra*-T2A-Cre colony backcrossed to C57BL/6 mice for 6 generations were analyzed at the age of 7–12 weeks. In Figures 6E, 6G, 6H, and S6G–S6I, the mice backcrossed to C57BL/6J mice for 6 generations were analyzed at the age of 8–19 weeks (Figures 6E, 6G, 6H, and S6G) and 12–23 weeks (Figures S6H and S6I). In Figures 6E, 6G, 6H, and S6G, the control R26CAG-FLEX-hM3Dq or *Il31ra*-T2A-Cre mice were littermates of the *Il31ra*-T2A-Cre R26CAG-FLEX-hM3Dq mice. In Figures 6J and 6K, the wild-type mice from the Nav1.8-Cre colony backcrossed to C57BL/6 mice for 5 generations were analyzed at the age of 9–15 weeks. In Figure S6J, S7–S10 weeks old male and female C57BL/6 mice were analyzed.

Figures 7 and S7: The mice backcrossed to C57BL/6J mice for 5 generations were analyzed at the age of 6–16 weeks (Figure 7B), 8–12 weeks (Figures 7C–7K), and 8–10 weeks (Figures S7A and S7B). In Figure 7B, the control mice had the genotypes of *Stat3*$^{fl/fl}$ and

were littermates of the Nav1.8-Cre *Stat3*$^{fl/fl}$ mice. In Figures S7A and S7B, the control Nav1.8-Cre R26CAG-floxStop-tdTomato mice and Nav1.8-Cre *Stat3*$^{fl/fl}$ R26CAG-floxStop-tdTomato mice were not littermates but were from the same colonies.

METHOD DETAILS

Immunofluorescence staining of DRG sections

Mouse DRGs were fixed in 4% paraformaldehyde (PFA; Fujifilm Wako Chemicals) in PBS (pH 7.4) at 4°C for 1 h, washed in PBS at 4°C for at least 1 h, embedded in Tissue-Tek O.C.T Compound (Sakura Finetek), and snap-frozen in dry ice and ethanol. Cryosections with 14 μm thickness on MAS-GP-coated glass slides (Matsunami Glass) were blocked in the blocking buffer containing 5 mg/mL BSA, 0.3% Triton X-100, and 5% normal donkey serum (Jackson ImmunoResearch) in PBS for 30 min at room temperature. The sections were then incubated with the primary antibodies as below in the blocking buffer for 3 h at room temperature and washed with the wash buffer (2 mg/mL BSA and 0.1% Triton X-100 in PBS) for 2 h. Then, the sections were incubated with the secondary antibodies as below in the blocking buffer for 1 h, washed with the wash buffer for 2 h, and mounted with Fluorescence mounting medium (DAKO). The primary antibodies were goat IgG anti-IL-31RA polyclonal antibody (pAb) (R&D Systems, AF2107, 1:500), goat IgG anti-GFRA1 pAb (R&D Systems, AF560, 1:200), goat IgG anti-GFRα2 pAb (R&D Systems, AF429-SP, 1:200), rat IgG anti-OSMR monoclonal antibody (mAb) (MBL, clone 30-1, 1:200), mouse IgG2a anti-beta III tubulin mAb (1:500), and rabbit IgG anti-pSTAT3 (Tyr705) pAb (Cell Signaling, 9145S, 1:200). The secondary antibodies were Alexa Flour 488-, 555- or 647-conjugated donkey anti-goat IgG pAb (Thermo Fisher Scientific; A-11055, A-21432, A-21447; 1:500), Alexa Flour 488-conjugated donkey anti-rat IgG pAb (Thermo Fisher Scientific, A-21208, 1:500), Alexa Flour 488-conjugated rat anti-mouse IgG2a pAb (Abcam, ab172324, 1:500), or Alexa Flour 488- and 647-conjugated Donkey anti-rabbit IgG pAb (Thermo Fisher Scientific; A-21206, A-31573; 1:500).

Whole mount immunofluorescence staining of ear skin tissues

Mouse ear pinnae were harvested and split into dorsal and ventral layers. The ventral layer with the cartilage was fixed in 4% PFA at 4°C for 1 h and then washed in PBS for at least 12 h. After the cartilage was removed under a stereo microscope using tweezers, the ear tissue was blocked with the blocking buffer containing 5 μg/mL anti-CD16/CD32 (BD Biosciences, clone 2.4G2), 5 mg/mL BSA, 0.3% Triton X-100, 5% normal donkey serum, and 5% normal rat serum (Jackson ImmunoResearch) in PBS at 37°C for 18 h, and then incubated with the primary antibodies as below in the blocking buffer at 37°C for 18 h. After washing with the wash buffer (2 mg/mL BSA and 0.1% Triton X-100 in PBS) at 37°C for 6 h (2 h × 3 times), the tissues were stained with the secondary antibodies as below in the blocking buffer at 37°C for 18 h. After washing with the wash buffer at 37°C for 4 h, the tissues were stained with 3.5 μM DAPI (Dojindo, D523) in the wash buffer at 37°C for 1 h, washed again for 1 h, and mounted in Fluorescence mounting medium (DAKO). The primary antibodies were goat IgG anti-IL-31RA pAb (R&D Systems, AF2107, 1:100), mouse IgG2a anti-beta III tubulin mAb (Abcam, ab78078, clone 2G10, 1:500), and rabbit IgG anti-RFP pAb (MBL, PM005, 1:500). The secondary antibodies were Alexa Flour 647-conjugated donkey anti-goat IgG pAb (Thermo Fisher Scientific, A-21447, 1:500), Alexa Flour 488-conjugated rat anti-mouse IgG2a pAb (Abcam, ab172324, 1:500), and Alexa Flour 555-conjugated donkey anti-rabbit IgG pAb (Thermo Fisher Scientific, A-21432, 1:500).

Confocal microscopy and image analysis

DRG section and whole-mount ear skin images were obtained using the TCS SP8 confocal microscope operated by the LAS X software, version 3.5.7.23225 (Leica Microsystems). Specimens were scanned sequentially with a 405-nm diode laser, a 488-nm optically pumped semiconductor laser (OPSL), a 552-nm OPSL, and a 638-nm diode laser. Emission signals were collected by using a 414–448-nm emission filter for DAPI; a 498-538nm emission filter for Alexa Flour 488 or GFP; a 555-597nm emission filter for Alexa Flour 555, tdTomato or mCherry; and a 653–800-nm emission filter for Alexa Flour 647. DRG section images were acquired using HC PL APO CS2 20×/0.75 dry. Each *x-y* plane was scanned twice at a resolution of 0.28 × 0.28 μm/pixel (the dwell time per pixel for each laser: 0.60 μs), and averaged images were obtained. For each z stack of DRG images, 11-15 *x-y* plane images with 1 μm z-spacing were obtained. Whole-mount ear skin images were acquired using HC PL APO CS2 40×/1.30 OIL lens. Each *x-y* plane image was obtained by scanning at a resolution of 0.28 × 0.28 μm/pixel (the dwell time per pixel for each laser: 1.2 μs). For each z stack of skin images, 55-134 *x-y* plane images with 0.5 μm z-spacing were obtained. Confocal image stacks were volume-rendered and analyzed using the Imaris 10.0.0 software (Oxford Instruments). Cubic regions were made (10^3 μm^3) on DAPI-positive nuclei, and mean fluorescence intensities of pSTAT3 staining signals were obtained for individual cubic regions. pSTAT3$^+$ neurons in DRGs from MC903-treated mice were determined as neurons with higher pSTAT3 staining signals than the highest pSTAT3 staining signals of neurons in DRGs from ethanol-treated control mice.

Bulk cell sorting from ear skin tissues

To prepare single cell suspensions from the ear skin, the ears were split into dorsal and ventral layers and digested with 0.5 mg/mL Liberase TL (Roche) and 0.2 mg/mL DNase I (Roche) at 37 c for 2 h before passing through 70-μm nylon strainers (BD Falcon). Cells were resuspended in PBS with 1% FBS, 2 mM EDTA, and 2.5 μg/mL anti-CD16/CD32 mAb (BD Biosciences, clone 2.4G2), and then stained with the fluorescent antibodies and LIVE/DEAD Fixable Aqua Dead Cell Stain Kit (Thermo Fisher Scientific). CD4$^+$ T cells were sorted using BD FACSAria III with with the 85-μm nozzle and BD FACSDiva software, version 6.1.1 (BD Biosciences). The data were

analyzed using FlowJo software (Tree Star). The fluorescent antibodies were PE-conjugated anti-CD3ε mAb (BD Biosciences, clone 17A2, 1:400), APC-conjugated anti-CD4 mAb (Biolegend, clone GK1.5, 1:200), APC-Cy7-conjugated anti CD45.2 mAb (Biolegend, clone 104, 1:200). See Figure S2 for the gating strategy. The ear skin from 10 ethanol-treated mice and 1 MC903-treated mouse was used for cell sorting to prepare each sorted cell sample containing at least 40,000 CD45-negative cells, 4,000 $CD45^+$ $CD3\varepsilon^+$ $CD4^+$ T cells, or 70,000 other $CD45^+$ luekocytes.

Bulk cell sorting from DRGs

DRGs were harvested and incubated in the digestion buffer containing 0.5 mg/mL liberase TL (Roche), 5 mg/mL dispase II (Sigma), 0.33 mg/mL papain (Sigma) and 0.1 mg/mL DNase I (Roche) in D-MEM (High Glucose) with L-Glutamine and Phenol Red (Fujifilm Wako Chemicals) supplemented with 10 μM 2-ME at 37°C for 10 min. Samples are gently pipetted several times using glass Pasteur pipettes and incubated for further 10 min at 37°C. EDTA was added to make the final EDTA concentration of 5 mM for termination of the digestion reaction. Samples are passed through 70-μm nylon strainers (BD Falcon) and resuspended in D-MEM (High Glucose) with L-Glutamine and Phenol Red supplemented with 10 μM 2-ME and 1% FBS. Nav1.8-tdTomato$^+$ cells were sorted using BD FACS Aria III with the 130-μm nozzle. C1-8 and T1-13 DRGs (42 DRGs on the both sides of the spinal cord) from each mouse were used to prepare each sorted cell samples containing at least 8,000 Nav1.8-tdTomato$^+$ cells.

RT-qPCR

Epidermal sheets were prepared as described previously.[50] Lysate preparation and RNA extraction from tissue samples were performed as described in the previous study.[21] Each tissue lysate sample contained 6 C1-C3 DRGs or an epidermal sheet isolated from the ventral side of an ear pinna. For RNA extraction from sorted cells, each sample contained 40,000–100,000 CD45-negative cells, 4,000–23,000 $CD45^+$ $CD3\varepsilon^+$ $CD4^+$ T cells, 70,000–100,000 other $CD45^+$ leukocytes, or 8000–10000 Nav1.8-tdTomato$^+$ sensory neurons. Total RNA was extracted from each sample by using 1 mL of TRIzol Reagent and 0.2 mL chloroform. After extraction, RNA from each sample was precipitated by adding 20 μg glycogen (GeneMark, GM14) and 0.5 mL isopropanol, washed with 70% ethanol, and dissolved in 10–20 μL DEPC-treated water (Nacalai, 36415-54). RNA was reverse-transcribed into cDNA by using High-Capactiry cDNA reverse transcription kit (Applied Biosystems). The target gene amplification using the below primers were quantified by using Fast SYBR Green Master Mix (Applied Biosystems) and StepOnePlus Real-Time PCR System (Thermo Fisher Scientific). Cycle threshold values were converted to theoretical expression values (2^{CT}), which were then normalized relative to *Gapdh* or *Hprt* expression. The primers for CD45-negative cells, $CD45^+$ $CD3\varepsilon^+$ $CD4^+$ T cells, and other $CD45^+$ luekocytes were *Gapdh* Forward (5′-AATGGTGAAGGTCGGTGTGA-3′), *Gapdh* Reverse (5′-AATCTCCACTTTGCCACTGC-3′), *Il31* Forward (5′-GCCCCAATATC GAAGGAAGA-3′), *Il31* Reverse (5′-CCAGATGCCTGCTTTATGCT-3′), *Il4* Forward (5′-CAAACGTCCTCACAGCAACG-3′), and *Il4* Reverse (5′-ATAAAATATGCGAAGCACCTTGG-3′). The primers for Nav1.8-tdTomato$^+$ cells were *Hprt* Forward (5′- ATGATCA GTCAACGGGGGAC-3′), *Hprt* Reverse (5′-TTATAGTCAAGGGCATATCC-3′), *Il31ra* Forward (5′- TTGGCACTGTGGGCATTCTC-3′), *Il31ra* Reverse (5′- GAGCTTGTACTTCAACACTGCAG-3′), *Osmr* Forward (5′-GTCACAACTCCAGATGCACG-3′), *Osmr* Reverse (5′-GTTTCCCAGAGCCTACACAC-3′), *Nppb* Forward (5′-CCAGAGCAATTCAAGATGCAGAAGC-3′), *Nppb* Reverse (5′-GTGCGTTA CAGCCCAAACGACT-3′), *Sst* Forward (5′-CAGACTCCGTCAGTTTCTGC-3′), *Sst* Reverse (5′-CAGGATGTGAATGTCTTCCAG-3′), *Mrgprd* Forward (5′-TGGCTGGGAGCAGTAGAGAC-3′), *Mrgprd*-Reverse (5′-CCATGGTGGGACTGATGGTC-3′).

In vivo treatments

For MC903 treatments, mice were anesthetized and 2 nmol MC903 (Cayman Chemical) in 100% ethanol was topically applied to the ear skin once a day for 7 consecutive days. For scratching analysis after s.c. injections, mice were held and restrained in a hand without anesthesia and s.c. injected with 2 μg recombinant mouse IL-31 (Rockland), 100 μg compound 48/80 (Sigma-Aldrich), 40–400 μg chloroquine diphosphate salt (Sigma-Aldrich), 5–50 μg Histamine (Sigma-Aldrich), or 4.5–112.5 μg Clozapine N-oxide (Cayman Chemical) in 50 μL PBS at the nape. mLTC4 (Cayman Chemical) was dissolved in ethanol at 100 μg/mL and diluted in PBS, and 0.3–0.75 μg mLTC4 in 50 μL was s.c. injected at the nape. The STAT3 antagonist S3I-201 (Sigma-Aldrich) was dissolved in DMSO at 25 mg/mL and further diluted in corn oil (Sigma-Aldrich) to 1.25 mg/mL for i.p. injections at 10 mg/kg mouse weight.

Scratching behavior analysis

Scratching movements of the hind paws were detected and analyzed using the MicroAct system (Neuroscience). Mice were anesthetized with 3–5% isoflurane and small Teflon-coated magnets (1mm diameter, 3mm long) were implanted into the dorsum of both hind paws at least 2 days before the experiment. The experimental mice were placed in observation chambers, each of which sat in the middle of a circular coil. Electric currents induced by movements of the magnets were recorded and transformed into the visual scratching waves by the MicroAct software. The following analysis conditions in the software were used to exclude hind paw movements that were not of scratching: bouts longer than 0.2 s, more than 3 strokes per bout, and peak range of 0.1–2.5 s. The analysis parameters are: duration, beats (scratching strokes) and bouts (number of events). Behavior of the mice was also recorded during the MicroAct measurements by video cameras placed over the observation chambers, and scratching bouts detected by the MicroAct system were visually verified.

Single cell sorting of DRG neurons for scRNA-seq

DRGs were processed as described above for bulk cell sorting from DRGs. Each of single Nav1.8-tdTomato$^+$ cells was sorted using BD FACS Aria III with the 130-μm nozzle into each tube of 8-well PCR Tube Strips 0.2 mL with Cap Strips (Nippon Genetics) containing 0.4 μL per tube of 10 × SingleCellProtect Single Cell Stabilizing Solution (Avidin Biotechnology) and immediately frozen in liquid nitrogen. A total of 400 cells were collected from 6 mice.

scRNA-seq

Digital RNA sequencing[51,52] was performed for the collected 400 cells. Library of each single cell was generated as previously described.[53] The libraries were sequenced with different sample indexes by HiSeq 2500 (Illumina, Rapid SBS Kit v2 and PE Rapid Cluster Kit v2). Sequencing data were mapped against mouse genome (mm10 assembly from the UCSC Genome Browser) with mouse gene annotation (refFlat from the UCSC Genome Browser) using STAR ver.2.7.3a.[54] The detected number of molecules for each gene per cell was counted based on molecular barcodes.[53] The number of molecules for each gene per cell was calculated using the detection efficiency of the spike-in RNAs which were measured together with every cell (total input number of spike-in RNA molecules per cell: 39000). In this process, six cells which had $\leq$1000 molecules of detected spike-in RNAs were removed. All sequencing datasets have been deposited in the Genome Expression Omnibus database under accession no. GSE218900.

Unsupervised clustering analysis using seurat package

The calculated numbers of molecules for genes per cell were imported into the Seurat (v2.3.4) R package.[46] Cells with 3000 unique genes or less were removed, which reduced the number of cells from 400 to 357 (Figure 3B). For the remaining cells, the data were normalized and scaled, and the PCA analysis was performed. Based on the principal components identified, unsupervised clustering analysis was performed using the graph-based clustering approach, which divided the cells into 5 distinct clusters. Using the Seurat package, the markers which define each cluster were compared with subset specific genes in the previous study.[13] Non-linear dimensional reduction was performed to generate tSNE plots using ggplot2 package (v3.1.0).

QUANTIFICATION AND STATISTICAL ANALYSIS

Data representation and statistical calculations were carried out using Prism software version 9 (GraphPad Software, La Jolla, CA). Probabilities were determined by two-tailed Student's t test for the comparison of two group means and by one-way ANOVA with Bonferroni's post-test for the comparison of more than two group means.